BRILLOUIN SCATTERING IN ZnSe

by

Clifford Gerald Hodgins

B.Sc. (Honors), Simon Fraser University, 1972

A THESIS SUBMITTED IN PARTIAL FULFILLMENT OF

THE REQUIREMENTS FOR THE DEGREE OF

MASTER OF SCIENCE

in the Department

of

Physics

SIMON FRASER UNIVERSITY

May 1974

APPROVAL

Name: Clifford Gerald Hodgins

Degree: Master of Science

Title of Thesis: Brillouin Scattering in ZnSe

Examining Committee:

Chairman: R. F. Frindt

J. C. Irwin
Senior Supervisor

A. E. Curzon

L. H. Palmer

E. D. Crozier

Date Approved: May 30/74

ABSTRACT

A Brillouin scattering apparatus has been constructed and measurements performed on the II-VI semiconductor ZnSe. In the experiments a single mode of the 514.5 nm line of an argon-ion laser was used as the light source and a molecular iodine filter was used to resolve the Brillouin components in the presence of a strong Rayleigh component. An analysis of the spectra has provided the following values for the elastic constants of single-crystal ZnSe: $C_{11} = 87.2 \pm 0.6$, $C_{12} = 52.4 \pm 0.8$ and $C_{44} = 39.2 \pm 0.4$ in units of 10^{10}dyne/cm^2. The present results were compared to previous piezo-resonance and ultrasonic measurements and also to values determined from neutron data. In addition, comparisons were made with the elastic moduli of polycrystalline ZnSe and further, an estimate was made of the relative magnitude of the photoelastic coefficients.

Acknowledgements

I wish to acknowledge the generous assistance given to me by my supervisor, Dr.J.C. Irwin, to whom I am indebted. Thanks are due the members of this department for their friendly cooperation. Special thanks to my colleagues R.M. Hoff, J.L. LaCombe, P.J. Joensen, I.S. Gordon and T.A. McMath for the many valuable discussions and for the assistance so generously given over these past few years. The financial support of the National Research Council of Canada is gratefully acknowledged. Finally, I wish to express deep appreciation to my parents for their support and encouragement during this period of thesis research.

Table of Contents

List of Tables

List of Figures

CHAPTER 1

INTRODUCTION

1.1 Preface

The long wavelength acoustic vibrations of dielectric crystalline solids have been investigated in the past by various methods. These methods include ultrasonic techniques (Huntington, 1947, 1958), piezo-resonance techniques (Cady, 1964), neutron scattering experiments (Batchelder et al., 1970) and Brillouin scattering measurements (Gornall et al., 1971). The results of such experiments provide information on the velocity of sound (elastic moduli), photoelastic constants and piezoelectric coefficients of the crystal. In addition, if the measurements are made as a function of frequency the long wavelength dispersion of the acoustic phonon branches can be determined. This information is of course not only of direct interest, as it pertains to the properties of the crystal, but is important as a basis for any theoretical analysis of the vibrational spectrum. A brief discussion of the merits of the above techniques is given in the following sections.

1.2 Ultrasonic Methods

Ultrasonic techniques are used to generate long wavelength acoustic vibrations in crystalline solids. Transducers

are used to excite the longitudinal and transverse elastic waves at frequencies up to about 10^8 Hz. The sound velocity is determined from the time taken for the impressed pulse to travel through a known crystal dimension and the elastic constants are then determined from these measured sound velocities (Fedorov, 1968). Using pulse-echo techniques, as outlined by McSkimin (1950, 1961), the sound velocities can be determined to within .1%.

Due to their poor performance at higher frequencies transducers are limited in operation to frequencies $\lesssim 10^8$ Hz and as a result only acoustic phonons within this rather limited frequency range can be investigated. Furthermore, the requirement of sufficiently large samples ($\sim$1 cm^3) limits the range of available crystals. A discussion of the experimental technique is given by Huntington (1947, 1958).

1.3 Piezo-Resonance Techniques

The piezo-resonance technique, also known as the resonance or dynamic method, uses the response of a piezoelectric crystal to an alternating electric field to determine the elastic and piezoelectric constants. The specially cut piezoelectric crystal is oriented in an external electric field in such a manner as to excite the desired vibrational mode. The applied electric field produces a deformation of the crystal through the action of the converse piezoelectric effect and,

as a result of the direct effect, this deformation induces a polarization in the crystal. This polarization, in turn, has an associated electric field whose reaction on the external field can be monitored. When the frequency of the applied field corresponds to a normal vibrational mode of the crystal the amplitude of the deformation reaches a maximum. This resonance can be observed by monitoring the current in the driving circuit. This current is maximized at resonance. The measured resonant and anti-resonant frequencies of the driving field can be related directly to the elastic, piezoelectric and dielectric constants of the crystal (Cady, 1964; Berlincourt et al., 1964; Mason, 1950).

This technique has the advantage in that it provides a measure of the dielectric constants as well as the elastic and piezoelectric coefficients. This method is further useful in determining the effect of external influences, such as temperature and pressure, on these parameters. Also, due to the present interest in piezoelectric devices much technical information exists on the piezoelectric effect.

In this technique typical resonant frequencies occur in the range of .1 ~ 50 MHz and thus only very low frequency phonons are sampled. Also, the elastic constants determined by this method have an uncertainty of about 1-2%; due mainly to the complex mathematical analysis required and uncertainty

in the dimensional measurements of the crystal samples. The method requires rather large crystals (.1 cm × 1 cm ×1 cm) usually in the form of a parallelepiped. The analysis of the data with different field orientations is naturally simplified if the external field is applied along a symmetry axis of the crystal and becomes increasingly complex as other orientations are used. Furthermore, this method is only applicable to piezoelectric crystals.

1.4 Neutron Scattering

A direct measure of phonon dispersion throughout the Brillouin zone is provided by neutron scattering (Leake et al., 1969; Hennion et al., 1971). Thermal neutrons from a reactor have energies and wavelengths comparable to those of the vibrational frequencies and lattice spacings, respectively. The energy change of the neutron as a function of scattering angle can be used to determine the frequency and wavelength of the lattice vibrations. However, due to insufficient energy resolution and small fluxes it is difficult to analyze the scattering from long wavelength acoustic phonons.

Alternatively, an interatomic force constant model is usually used to fit a theoretical dispersion curve to the data. The model has several parameters which are determined from measured phonon frequencies and the model is then used to determine the elastic constants from the slope of the acoustic branches in the long wavelength limit.

Since neutron beams are not intense large crystal volumes (~1 cm^3) and long counting times are required. Some materials are not suited for this method because of their high neutron absorption or large incoherent scattering cross-sections. Also, the elastic constants determined from the neutron data may differ significantly from those determined by more direct methods (Irwin and LaCombe, 1972). On the other hand neutron data does provide valuable information about phonon dispersion and when used with other measurements can provide an accurate indication of dispersion throughout the Brillouin zone.

1.5 Brillouin Scattering

The invention of the laser renewed interest in the phenomena of the scattering of light by crystal lattice vibrations first proposed by Brillouin (1914, 1922). This method serves to complement that of ultrasonics in that it enables one to extend the measured phonon frequencies to the gigahertz.

In Brillouin scattering laser light is incident on a sample and the scattered light is frequency analyzed. The light is scattered due to fluctuations in the polarizability tensor. These fluctuations are generated by the thermal sound waves in the medium. From an analysis of the spectrum of the scattered radiation the phase velocity of the sound waves can be measured and the elastic constants determined.

Essentially there are no restrictions on crystal size or type other than that the crystal transmit a portion of the exciting light. Phonon phase velocities can be determined for practically any crystallographic direction but the more symmetric directions naturally provide the simplest relations between phase velocity and elastic constants. The relative ease of applying Brillouin scattering measurements in various scattering geometries can result in more information about phonon dispersion than from either ultrasonic or piezo-resonance methods. However, the experimental uncertainty associated with phase velocity measurements in Brillouin scattering is usually about 1% as compared to .1% for ultrasonic methods; due primarily to a lack of angular resolution associated with the former. A review of the Brillouin scattering technique is given by Benedek and Fritsch (1966) and an outline of their analysis is presented in Chapter 2 of this thesis.

From this discussion it can be concluded that Brillouin scattering is a versatile method for obtaining sound velocities and complements ultrasonic and piezo-resonance measurements. However, in the past Brillouin scattering experimentation in solids has been complicated by the large amount of light scattered at the unshifted laser frequency. This unshifted component will hereafter be referred to as the Rayleigh component. The intensity of this central component was

4 to 5 orders of magnitude larger than that of conventional Rayleigh scattering. This increased scattering was mainly due to scattering from crystal imperfections and the collection of specularly reflected light from the crystal faces. This component may be so intense that the instrumental "wings" are not sufficiently rejected by the experimental apparatus and as a result the Brillouin components cannot be resolved. This problem is particularly severe in solids with a large refractive index due to the enhanced reflections from such crystals; as for example the ZnSe crystals used in the present experiment.

This problem has been overcome by using a molecular iodine filter as proposed by Devlin et al.(1971) to attenuate the 5145 Å single mode output of an argon-ion laser. This arrangement should now make the technique of Brillouin scattering applicable to an extremely wide range of solids and in particular to wide band semiconductors of the II-VI and III-V groups where large single crystals are hard to obtain.

1.6 Present Work

Due to our interest in II-VI semiconductors it was decided to construct an apparatus for performing Brillouin scattering measurements. The assembly and experimental method of such an apparatus is described in Chapter 3 of this thesis. An evaluation of the apparatus and method is given in Chapter 4 where measurements were performed on crystalline α-Quartz for which the elastic constants are well known (McSkimin, 1962; Cecchi et al., 1970).

The primary aim of this experiment was, however, to measure the elastic constants of Zinc Selenide (ZnSe). The elastic constants were first determined by Berlincourt et al. (1963) from piezo-resonance data. A more recent ultrasonic measurement by Lee (1970) produced values which disagreed with Berlincourt's. Furthermore, on the basis of his neutron results Hennion et al. (1971) suggested that Berlincourt's results were grossly in error. This suggestion was reinforced by Talwar et al. (1972) on the basis of an interpretation of the neutron data using a seven parameter model called the second neighbour ionic (SNI) model (Banerjee and Varshni, 1969).

Due to the large discrepancies between these sets of data it was decided that an independent measurement was warranted. The method of Brillouin scattering was chosen since it seemed the most appropriate, especially due to the small crystal samples available and further because of the recent discovery (Devlin et al., 1971) of the molecular iodine filter.

Furthermore, this technique would complement the previous measurements by extending the phonon frequencies to the gigahertz range, thus providing an indication of any serious dispersion in the acoustic phonon branches near $\underline{K} = 0$.

The results of the Brillouin scattering measurements are presented in Chapter 5 where a comparison is made to the

previous experimental results. In particular, the present work is compared to the measurements of Berlincourt et al. (1963), Lee (1970) and the neutron results of Hennion et al. (1971) and Talwar et al. (1972). In addition, a comparison is made to the polycrystalline elastic moduli of ZnSe (Chung et al., 1967) and a discussion of the consistency of the data is made using a relation due to Martin (1970). Finally, the present data is used to estimate the relative magnitude of the photoelastic coefficients.

CHAPTER 2

THEORY

2.1 Introduction

In the first part of this chapter the theory of Brillouin scattering in cubic crystals is presented. The analysis follows that given by Benedek and Fritsch (1966). Results for the scattered field and spectral density function are derived and a weighting factor is defined for the scattered intensity. In the second part a theory of elastic waves in cubic crystals, due to Fedorov (1968), is used to determine the relation between the sound velocity and the elastic constants. Finally, relationships between the Brillouin frequency shifts and the elastic constants are derived (Tables I-V) for the various scattering geometries used in the present experiment.

2.2 Brillouin Scattering

Brillouin scattering refers to the scattering of light by long wavelength acoustic phonons. The scattering results from interactions between the incident electromagnetic field and propagating thermal fluctuations in the medium. These thermal fluctuations cause a local change in the polarizability or dielectric constant and the scattering can be analyzed in terms of these thermally generated fluctuations.

Such an analysis follows from the identification (Debye, 1912) of the thermal content of the medium with the excitation of crystal lattice vibrations. The connection between the sound wave and the fluctuations in the dielectric constant was derived by Pockels (1906). In his analysis Pockels related the fractional change in the dielectric tensor to the strain tensor components of the sound wave. The fluctuating component of the dielectric tensor causes the incident radiation to be scattered.

The scattering may also be viewed classically as "Bragg" reflection from fluctuations whose wavelength (λ_f) and scattering angle (θ) are related to the wavelength of the exciting radiation in the medium ($\frac{\lambda_o}{n}$) by the Bragg condition:

$$\frac{\lambda_o}{n} = 2\lambda_f \sin(\frac{\theta}{2}) \qquad (2.1)$$

where n is the index of refraction of the medium. Alternatively, the scattering may be viewed as a doppler shift in frequency of the incident radiation due to propagating dielectric fluctuations of phase velocity V_s. The corresponding fractional shift in frequency is given by the Brillouin formula:

$$\frac{\Delta\nu}{\nu_o} = \frac{-\Delta\lambda}{\lambda_o} = \frac{2nV_s \sin(\frac{\theta}{2})}{C} \qquad (2.2)$$

where C is the velocity of light in vacuum. This formula

was first obtained by Brillouin (1914, 1922) and shows that the spectrum of the scattered light can provide a determination of the phase velocity of thermally excited sound waves whose wavelength is of the same order as that of the detecting radiation. Such sound waves have frequencies of the order of 1 - 50 GHz in solids.

Early theories of Brillouin scattering were made by Brillouin (1914, 1922) and Landau and Placzek (1934). More recent theories were formulated by Pecora (1964) and Mountain (1966). In these later treatments the spectrum of the scattered light was related to the space-time correlation function for the density fluctuations in the scattering medium. A classical treatment appropriate to crystalline solids has been given by Benedek and Fritsch (1966) and an outline of their analysis is presented here.

2.3 Scattering Amplitude

In this section an expression for the amplitude of the scattered field is derived. Scattering of the incident radiation arises from the presence of a fluctuating component in the polarizability tensor of the medium. The polarization $\underline{P}(\underline{r},t)$ at $\underline{r}$ gives rise to a scattered field $d\underline{E}'(\underline{R},t)$ at the field point $\underline{R}$ and time t:

$$d\underline{E}'(\underline{R},t) = \left[\frac{\hat{\ell}_{\underline{R}-\underline{r}} \times \left(\hat{\ell}_{\underline{R}-\underline{r}} \times \ddot{\underline{P}}(\underline{r},t') \right) |d\underline{r}|}{C^2 |\underline{R}-\underline{r}|} \right]_{t'=t-\frac{|\underline{R}-\underline{r}|}{C_n}} \qquad (2.3)$$

where the vectors $\underline{R}$, $\underline{r}$ and the unit vectors $\hat{\ell}_{\underline{R}-\underline{r}}$ and $\hat{\ell}_k$ are shown in Figure 1.

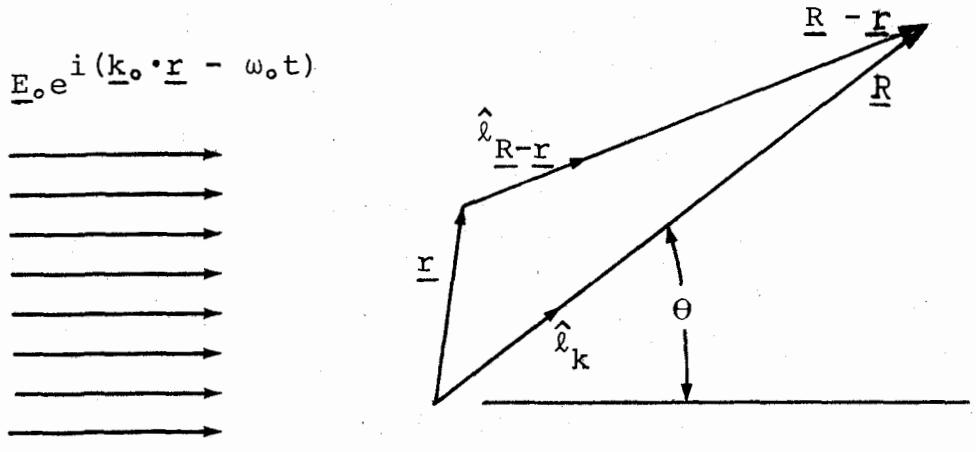

Figure 1. The Scattering Geometry

For simplicity the field point $\underline{R}$ is taken within the medium, the exterior field given by the general laws of reflection and refraction. In equation 2.3, t' is the retarded time $(t - \frac{|\underline{R}-\underline{r}|}{C_n})$ calculated using the velocity of light in the medium $(C_n = C/n)$.

The macroscopic polarizability tensor $\underset{\sim}{\alpha}(\underline{r},t)$ may be written as the sum of a time averaged part $\langle\underset{\sim}{\alpha}(\underline{r},t)\rangle$ and a fluctuation $\delta\underset{\sim}{\alpha}(\underline{r},t)$. The dielectric tensor is related to the polarizability tensor according to:

$$\underset{\sim}{\alpha}(\underline{r},t) = \frac{\underset{\sim}{\varepsilon}(\underline{r},t)-1}{4\pi} = \frac{\langle\underset{\sim}{\varepsilon}(\underline{r},t)-1\rangle}{4\pi} + \frac{\delta\underset{\sim}{\varepsilon}(\underline{r},t)}{4\pi} \qquad (2.4)$$

where $\delta\underline{\underline{\epsilon}}(\underline{r},t) = \delta\underline{\underline{\xi}}(\underline{r},t)/4\pi$. Here the dielectric constant tensor $\underline{\underline{\xi}}(\underline{r},t)$ is written as the sum of a time averaged part $\langle\underline{\underline{\xi}}(\underline{r},t)\rangle$ and a fluctuation $\delta\underline{\underline{\xi}}(\underline{r},t)$ with tensor components $\delta\epsilon_{ij}(\underline{r},t)$.

The coupling between the thermal sound wave and the fluctuation in the polarizability is provided by the photoelastic (elasto-optic) coeffients P_{ijkl} (Pockels, 1906; Nye, 1957; Born and Huang, 1954):

$$\delta\epsilon_{ij}(\underline{r},t) = -\sum_{k,\ell=1}^{3} n_i^2\, n_j^2\, P_{ijk\ell}\, S_{k\ell}(\underline{r},t) \qquad (2.5)$$

where n_i is the component of the refractive index referred to the i-th coordinate axis and $S_{ij}(\underline{r},t)$ are the strain tensor components associated with the sound wave. The strain tensor components are defined to be:

$$S_{ij}(\underline{r},t) = \frac{1}{2}\left(\frac{\partial U_i}{\partial x_j} + \frac{\partial U_j}{\partial x_i}\right) \qquad (2.6)$$

where U_i is the i-th component of the displacement ($\underline{U}(\underline{r},t)$) of the atom at point $\underline{r}$ and time t and x_j refers to the j-th coordinate axis relative to which the tensor components $P_{ijk\ell}$ are defined.

In the special case of a cubic crystal there are only three non-zero photoelastic tensor components and equation 2.5 takes the form (Benedek et al., 1966; Nye, 1957):

$$-\frac{\delta\epsilon_{ij}(\underline{r},t)}{\epsilon_o^{\,2}} = 2P_{44}\,S_{ij}(\underline{r},t) + (P_{11}-P_{12}-2P_{44})\,\delta_{ij}\,S_{ii}(\underline{r},t) + P_{12}\left(\sum_{\ell=1}^{3} S_{\ell\ell}(\underline{r},t)\right)\delta_{ij} \qquad (2.7)$$

where δ_{ij} is the kronecker delta function and the reduced form of the photoelastic tensor has been used. The transformation $P_{ijk\ell} \rightarrow P_{\alpha\beta}$ has the same form as that for the elastic constants $C_{ijk\ell}$ (Appendix A; Fedorov, 1968). The reference coordinate axes employed here correspond to the four-fold rotational symmetry axes of the cubic lattice.

The polarizability at each point $\underline{r}$ in the medium can be written:

$$\underline{P}(\underline{r},t) = (\langle\underset{\sim}{\alpha}(\underline{r},t)\rangle + \delta\underset{\sim}{\alpha}(\underline{r},t)) \cdot \underline{E}_o\, e^{i(\underline{k}_o\cdot\underline{r}-\omega_o t)} \qquad (2.8)$$

To evaluate the second time derivative of $\underline{P}$ as required by equation 2.3 it should be remembered that the characteristic frequency for thermal fluctuations is $\lesssim 10^{12}$ Hz compared to the light frequency of about 10^{14} Hz. Thus $\delta\underset{\sim}{\alpha}(\underline{r},t)$ may be regarded as a slowly varying function of time and we may write:

$$\ddot{\underline{P}}(\underline{r},t) \cong -\omega_o^{\,2}\,\underline{P}(\underline{r},t) \qquad (2.9)$$

On substitution of equations 2.8 and 2.9 in equation 2.3 and integrating over the illuminated volume V at the retarded time t' we have for R>>r:

$$\underline{E}'(\underline{R},t) = -\left(\frac{\omega_o}{c}\right)^2 \frac{e^{i(\underline{k}_o' \cdot \underline{R} - \omega_o t)}}{R} \qquad (2.10)$$

$$\hat{\ell}_k \times \left(\hat{\ell}_k \times \iiint_V (\langle \underset{\sim}{\alpha}(\underline{r},t') \rangle + \delta\underset{\sim}{\alpha}(\underline{r},t')) \cdot \underline{E}_o \, e^{i(\underline{k}_o - \underline{k}_o') \cdot \underline{r}} \, |d\underline{r}| \right)$$

where $\hat{\ell}_{\underline{R}-\underline{r}} \cong \hat{\ell}_k$

$$\frac{n\omega_o}{c}|\underline{R} - \underline{r}| \cong \frac{n\omega_o}{c} \hat{\ell}_k \cdot (\underline{R}-\underline{r})$$

$$\underline{k}_o' = \frac{n\omega_o}{c} \hat{\ell}_k$$

and in the denominator $|\underline{R} - \underline{r}| \cong R$.

The volume integral in equation 2.10 represents the superposition of phases of waves scattered from each illuminated point in the medium. In the absence of the fluctuations $\delta\underset{\sim}{\alpha}$ this superposition leads to a complete cancellation of the scattered field. The contribution to the integral from the $\langle\underset{\sim}{\alpha}\rangle$ term is zero except in the forward direction ($\theta = 0$). Scattering out of the incident direction results entirely from fluctuations in the

polarizability.

The fluctuations in the polarizability tensor can be analyzed into spatial fourier components:

$$\delta\underset{\sim}{\alpha}(\underline{r},t') = \frac{1}{(2\pi)^{3/2}} \sum_{\mu} \iiint |d\underline{q}|\, \delta\underset{\sim}{\alpha}^{\mu}(\underline{q})\, e^{i(\underline{q}\cdot\underline{r} \mp \omega_{\mu}(\underline{q})t')} \tag{2.11}$$

where $\underline{q}$ and $\omega_{\mu}(\underline{q})$ are the wavevector and frequency of the fluctuation respectively. The index μ denotes the possibility of a number of branches in the dispersion relation $\omega(\underline{q})$ which correspond to the different phonon modes. In general $\omega_{\mu}(\underline{q})$ can be complex to include damping of the fluctuation. Also $\omega_{\mu}(\underline{q})$ is double valued ($\pm$) to account for degeneracy in the dispersion relation for positive and negative running waves.

The scattered field (2.10) can now be written using equation 2.11 as:

$$\underline{E}'(\underline{R},t) = -\left(\frac{\omega_o}{C}\right)^2 \sum_{\mu} \hat{\ell}_k \times \tag{2.12}$$
$$\left\{\hat{\ell}_k \times \iiint |d\underline{K}|\, (\delta\underset{\sim}{\alpha}^{\mu}(\underline{K})\cdot\underline{E}_o)\, e^{i(\underline{k}\cdot\underline{R} - (\omega_o \pm \omega_{\mu}(\underline{K}))t)}\right\}$$
$$\times (2\pi)^{3/2} \left[\frac{1}{(2\pi)^3} \iiint |d\underline{r}|\, e^{i(\underline{k}_o - \underline{k} + \underline{K})\cdot\underline{r}}\right]$$

where:

$$\underline{k} = \frac{n}{C}\,(\omega_o \pm \omega_{\mu}(\underline{K}))\ \hat{\ell}_k \tag{2.13}$$

is the scattered wavevector which corresponds to the scattering from a vibration of frequency $\omega_\mu(\underline{K})$.

The final integral in equation 2.12 is a delta function $[\delta(\underline{k}_o - \underline{k} + \underline{K})]$ provided the illuminated region is very large compared to the wavelength of the light. This merely expresses the conservation of momentum between the incident photon ($\underline{k}_o$), the scattered photon ($\underline{k}$) and the scattering fluctuation (crystal momentum) $\underline{K} = \underline{k} - \underline{k}_o$. It is emphasized that only the $\underline{K}$-th fourier component of the fluctuation contributes to the scattered field observed at the field point $\underline{R}$.

Substitution of equation 2.4 in 2.11 and relabelling $\underline{E}'(\underline{R},t)$ by $\underline{E}'(\underline{K},t)$ to emphasize the dependence on scattering wavevector ($\underline{K}$) equation 2.12 becomes:

$$\underline{E}'(\underline{K},t) = -\left(\frac{\omega_o}{C}\right)^2 \frac{(2\pi)^{3/2}}{4\pi R} \sum_\mu e^{i(\underline{k}\cdot\underline{R} - (\omega_o \pm \omega_\mu(\underline{K}))t)} \hat{\ell}_k \times \left[\hat{\ell}_k \times \left(\delta\underset{\sim}{\xi}^\mu(\underline{K})\cdot\underline{E}_o\right)\right] \qquad (2.14)$$

where it is noted that $\delta\underline{D}^\mu(\underline{K}) = \delta\underset{\sim}{\xi}^\mu(\underline{K})\cdot\underline{E}_o$ is the fluctuation in the displacement vector for the μ-th vibrational mode of wavevector $\underline{K}$.

The amplitude of the scattering from each branch (μ) is seen (2.14) to be proportional to that spatial fourier component of the fluctuation in $\underset{\sim}{\xi}$ which has wavevector

$\underline{K}$. The frequency of the scattered wave (ω') is shifted from the incident wave by an amount $\pm\ \omega_\mu(\underline{K})$. The scattered field contains peaks in amplitude at the frequencies $\omega_o \pm \omega_\mu(\underline{K})$. For a given phonon mode (μ) these peaks are referred to as the Brillouin doublets. The peak at $\omega_o - \omega_\mu(\underline{K})$ is called the Stokes component and that at $\omega_o + \omega_\mu(\underline{K})$ is called the anti-Stokes component.

2.4 Angular Dependence

The angular dependence of the Brillouin doublet spacing may be analyzed in the following manner. Let the incident light be scattered through an angle θ. Since the phonon energy is much less than that of the photon, the incident and scattered wavevectors are nearly of the same magnitude. Using conservation of momentum the phonon wavevector can then be given by:

$$K \cong 2k_o \sin(\frac{\theta}{2}) = \frac{2n\omega_o}{c} \sin(\frac{\theta}{2}) \qquad (2.15)$$

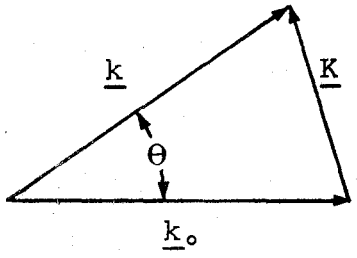

The corresponding frequency shift is determined

by the acoustic dispersion relation:

$$\omega_\mu(\underline{K}) = V(\mu, \hat{\ell}_K)K \tag{2.16}$$

where $\hat{\ell}_K = \underline{K}/K$ is the unit phonon wavevector. (Note: in this analysis the long wavelength limit is assumed).

Combining equations 2.15 and 2.16 the Brillouin formula (2.2) can be derived:

$$\frac{\omega'-\omega_o}{\omega_o} = \frac{\pm\omega_\mu(\underline{K})}{\omega_o} = \frac{\pm 2nV(\mu,\hat{\ell}_K)\ \sin\ (\frac{\theta}{2})}{C} \tag{2.2}$$

The dispersion relation (2.16) for acoustic phonons in solids contains in general three branches. These branches correspond to a longitudinal and two transverse vibrational modes. Thus there are three frequencies associated with the wavevector $\underline{K}$ and the Brillouin spectrum will in general contain three sets of doublets located "symmetrically" about the incident light frequency.

The derivation of the Brillouin formula (2.2) ignored the small change in the magnitude of the wavevector of the scattered radiation. A complete analysis has been given by Chandrasekharan (1965). The only modification is a slight asymmetry in the placement of the Brillouin doublets about the unshifted frequency ω_o. The correction $\delta\omega_\mu$ being towards higher frequencies for both Stokes and anti-Stokes components.

It can be shown that the fractional shift is: $\frac{\delta\omega_\mu}{\omega_\mu} = \frac{1}{2}\frac{\omega_\mu}{\omega_o}$. This fraction is approximately 10^{-6} for most solids and in the present experiment was too small an effect to be measurable.

2.5 Weighting Factor

In this section a weighting factor for the scattered field is defined. The weighting factor provides a measure of the amplitude of the scattered field and was found useful in predicting polarization selection rules in the scattering experiments.

The analysis of the scattered field (2.14) involved computing the fluctuation in the displacement vector $\delta\underline{D}^\mu(\underline{K})$. This requires a knowledge of the $\underline{K}$-th fourier component of the fluctuation in the dielectric tensor $(\delta\underline{\underline{\epsilon}}^\mu(\underline{K}))$. Taking the fourier transform of equation 2.7 and using equation 2.6 the following equations result:

$$-\frac{\delta\epsilon^\mu_{ij}(\underline{K},t)}{\epsilon_o^2} = 2\,P_{44}\,S^\mu_{ij}(\underline{K},t) + (P_{11}-P_{12}-2P_{44})\delta_{ij}\,S^\mu_{ii}(\underline{K},t) + P_{12}\Big(\sum_{\ell=1}^{3} S^\mu_{\ell\ell}(\underline{K},t)\Big)\delta_{ij} \qquad (2.17)$$

and

$$S^\mu_{\ell m}(\underline{K},t) = \frac{i}{2}(U^\mu_\ell(\underline{K},t)\,K_m + U^\mu_m(\underline{K},t)\,K_\ell) \qquad (2.18)$$

where we have included the mode index μ and assumed a travelling wave whose amplitude can be fourier analyzed into spatial components:

$$U_\ell^\mu(\underline{r},t) = \frac{1}{(2\pi)^{3/2}} \iiint |d\underline{q}| \; U_\ell^\mu(\underline{q},t)\, e^{i\underline{q}\cdot\underline{r}} \qquad (2.19)$$

where:

$$\underline{U}^\mu(\underline{K},t) = \underline{U}^{\mu'}(\underline{K})\, e^{\pm i\omega_\mu(\underline{K})t} \qquad (2.20)$$

Equation 2.20 represents the $\underline{K}$-th fourier component of the elastic displacement of the sound wave. The oscillatory character of the wave is contained in the exponential factor and $\underline{U}^{\mu'}(\underline{K})$ is assumed to contain a slow time dependence which corresponds to the decay of the sound wave due to viscous damping, thermal conduction and scattering from crystal defects.

Substitution of equations 2.17 and 2.18 in the definition of $\delta\underline{D}^\mu(\underline{K})$ (2.14) gives:

$$\delta\underline{D}^\mu(\underline{K}) = \frac{\epsilon_o^2}{i}\, U^{\mu'}(\underline{K})\, KE_o\, \underline{\rho}^\mu \qquad (2.21)$$

where the vector $\underline{\rho}^\mu$ is given by (Benckert and Bäckström , 1973):

$$\begin{aligned}\underline{\rho}^\mu = {} & P_{44}\left[\hat{\Pi}^\mu(\hat{\ell}_K\cdot\hat{\ell}_{E_o}) + (\hat{\Pi}^\mu\cdot\hat{\ell}_{E_o})\hat{\ell}_K\right] \\ & + P_{12}\left[\hat{\Pi}^\mu\cdot\hat{\ell}_K\right]\hat{\ell}_{E_o} \\ & + (P_{11} - P_{12} - 2P_{44})\sum_{\ell=1}^{3}(\hat{\Pi}^\mu)_\ell(\hat{\ell}_K)_\ell(\hat{\ell}_{E_o})_\ell\,\hat{1}_\ell \qquad (2.22)\end{aligned}$$

where $\hat{\Pi}^{\mu}$ is a unit vector in the direction of polarization of the sound wave. The components of $\hat{\Pi}^{\mu}$ along the cube axes are $(\hat{\Pi}^{\mu})_{\ell}$, $\ell = 1,2,3$. The unit vector $\hat{\ell}_K$ points in the direction of the sound wave and has components $(\hat{\ell}_K)_{\ell}$ along the cube axes. The unit vector $\hat{\ell}_{E_o}$ points in the direction of polarization of the incident light wave with components $(\hat{\ell}_{E_o})_{\ell}$ along the cube axes. $\hat{1}_{\ell}$ are unit vectors along the four-fold symmetry axes of the cubic lattice.

The direction and magnitude of vector $\underline{\rho}^{\mu}$ is determined by the vectors $\underline{K}$, $\underline{E}_o$ and $\hat{\Pi}^{\mu}$ and the magnitude of the photoelastic coefficients $P_{\alpha\beta}$. In general the electric displacement $\delta\underline{D}^{\mu}(\underline{K})$ is in a different direction from that of the incident field $(\underline{E}_o)$. Comparison with equation 2.14 reveals that we measure not $\underline{\rho}^{\mu}$ but the vector $\underline{\xi}^{\mu}$ which is related to $\underline{\rho}^{\mu}$ by:

$$\underline{\xi}^{\mu} = \hat{\ell}_k \times (\hat{\ell}_k \times \underline{\rho}^{\mu}) \qquad (2.23)$$

That is we measure the component of the displacement vector in the plane perpendicular to the scattered wavevector $(\underline{k})$. The factors $|\underline{\xi}^{\mu}|$ are called weighting factors since they determine the relative intensity of the light which is scattering from a phonon of mode μ.

The expression (2.14) for the scattered electric field can now be written using equations 2.20, 2.21 and 2.23 as:

$$\underline{E}'(\underline{K},t) = -\left(\frac{\omega_o}{C}\right)^2 \frac{(2\pi)^{3/2}}{4\pi R} \sum_{\mu} e^{i(\underline{k}\cdot\underline{R}-\omega_o t)}$$

$$\frac{\epsilon_o^2}{i} U^{\mu}(\underline{K},t)\ KE_o\ \underline{\xi}^{\mu} \qquad (2.24)$$

2.6 Spectral Distribution

The spectral distribution of the scattered radiation is best described by introducing the auto-correlation function for the scattered field:

$$\langle \underline{E}'(\underline{K},t+\tau) \cdot \underline{E}'^{*}(\underline{K},t) \rangle = \qquad (2.25)$$

$$\lim_{T\to\infty} \frac{1}{2T} \int_{-T}^{T} \underline{E}'(\underline{K},t+\tau)\cdot\underline{E}'^{*}(\underline{K},t)\ dt$$

The usual spectral density function $S(\underline{K},\omega')$ is then defined by:

$$S(\underline{K},\omega') = \frac{\frac{1}{2\pi}\int_{-\infty}^{\infty} \langle \underline{E}'(\underline{K},t+\tau)\cdot\underline{E}'^{*}(\underline{K},t)\rangle\ e^{i\omega'\tau} d\tau}{\langle |\underline{E}'(\underline{K},t)|^2 \rangle} \qquad (2.26)$$

which satisfies:

$$\int_{-\infty}^{\infty} S(\underline{K},\omega')\ d\omega' = 1. \qquad (2.27)$$

The total power radiated in all frequencies which is scattered into the solid angle $d\Omega$ at the field point $\underline{R}$ is proportional to the mean squared field strength and can be expressed as:

$$dP'(\underline{K},\underline{R}) = \frac{C}{8\pi} \langle |\underline{E}'(\underline{K},t)|^2 \rangle \, R^2 \, d\Omega \qquad (2.28)$$

Using equations 2.26, 2.27, and 2.28 the power scattered into the solid angle $d\Omega$ at the field point $\underline{R}$ which lies in the frequency interval between ω' and $\omega' + d\omega'$ is given by:

$$dP'(\underline{K},\omega') \, d\omega' = dP'(\underline{K},\underline{R}) \; S(\underline{K},\omega') \, d\omega' \qquad (2.29)$$

To determine the auto-correlation function (2.25) equation 2.24 can be used to derive the following expression:

$$\langle \underline{E}'(\underline{K},t+\tau) \cdot \underline{E}'^{*}(\underline{K},t) \rangle = \left(\frac{\omega_o}{C}\right)^4 \frac{\pi}{2} \frac{\epsilon_o^4}{R^2} K^2 E_o^2 \qquad (2.30)$$
$$\times \sum_{\mu=1}^{3} |\underline{\xi}^{\mu}|^2 \langle \underline{U}^{\mu}(\underline{K},t+\tau) \cdot \underline{U}^{\mu *}(\underline{K},t) \rangle \, e^{-i\omega_o \tau}$$

where it is remembered that sound waves belonging to different polarization branches are mutually orthogonal.

We call

$$\langle \underline{U}^{\mu}(\underline{K},t+\tau) \cdot \underline{U}^{\mu *}(\underline{K},t) \rangle$$

the auto-correlation function for $\underline{U}^{\mu}(\underline{K},t)$. This function may be obtained by reasoning along the following lines. In equation 2.20 the temporal dependence of the sound wave displacement

was broken into two parts. One contained the rapid sound oscillation ($e^{\pm i\omega_\mu(\underline{K})t}$) the other ($\underline{U}^{\mu'}(\underline{K},t)$) being the much slower statistical fluctuation of the amplitude factor. This amplitude factor is a random variable and is characterized by a temporal coherence with correlation time $\tau_\mu(\underline{K})$ and a correlation rate $1/\Gamma_\mu(\underline{K})$. Assuming that the correlation function for this amplitude is exponentially damped in time then:

$$\langle \underline{U}^{\mu}(\underline{K},t+\tau)\cdot\underline{U}^{\mu^*}(\underline{K},t)\rangle = \langle|\underline{U}^{\mu'}(\underline{K},t)|^2\rangle e^{\pm i\omega_\mu(\underline{K})\tau}\ e^{-\Gamma_\mu(\underline{K})\tau} \tag{2.31}$$

Physically $\Gamma_\mu(\underline{K})$ represents the decay rate for a sound wave of mode μ and wavevector $\underline{K}$.

The mean squared amplitude of the sound wave (2.31) can be related to the temperature (T) by the equipartition theorem for harmonic oscillators: the total vibrational energy is equal to twice the kinetic energy (K.E.):

$$\langle E\rangle = 2\langle K.E.\rangle = \left\langle \iiint |d\underline{r}|\rho|\dot{\underline{U}}(\underline{r},t)|^2 \right\rangle \tag{2.32}$$

where ρ is the mass density. Allowing for the double degeneracy in $\omega_\mu(\underline{K})$ for positive and negative running waves and using the fourier expansion of $\underline{U}(\underline{r},t)$ (2.19):

$$\langle E\rangle = 2\sum_\mu \iiint |d\underline{q}|\ \rho\omega_\mu^{\,2}(\underline{q})\ |\underline{U}^{\mu}(\underline{q})|^2 \tag{2.33}$$

Since $\underline{U}(\underline{q})$ are the normal coordinates for the lattice vibrations it is reasonable to denote $\langle E_\mu(\underline{q})\rangle$ as the thermal average of the energy for each normal mode. Using this correspondence the total energy can be written as the sum over all normal mode energies. This sum can be replaced by an integral over $|d\underline{q}|$ with an appropriate density of states function:

$$\langle E\rangle = \sum_\mu \iiint |d\underline{q}| \frac{V}{(2\pi)^3} \langle E_\mu(\underline{q})\rangle \tag{2.34}$$

where V is the volume of the solid. Comparing equations 2.33 and 2.34 and for $kT >> \hbar\omega_\mu$ (k is Boltzmann's constant) using $\langle E_\mu(\underline{q})\rangle = kT$ we find:

$$\langle |\underline{U}^\mu(\underline{K})|^2\rangle = \frac{V}{(2\pi)^3} \frac{kT}{2\rho\omega_\mu^2(\underline{K})} \tag{2.35}$$

Substitution of equation 2.35 in 2.31 gives the following expression for the correlation function (2.30):

$$\langle \underline{E}'(\underline{K},t+\tau)\cdot\underline{E}'^*(\underline{K},t)\rangle = E_o^2 \left(\frac{\omega_o}{C}\right)^4 \frac{\epsilon_o^4}{R^2} \frac{V}{(4\pi)^2}$$

$$\times \frac{kT}{2\rho} \sum_{\mu=1}^{3} |\underline{\xi}^\mu|^2 \frac{K^2}{\omega_\mu^2(\underline{K})} e^{-i(\omega_o \mp \omega_\mu(\underline{K}))\tau} \left(e^{-\Gamma_\mu(\underline{K})\tau}\right) \tag{2.36}$$

where it is remembered that the $\pm$ notation indicates a sum over both positive and negative running waves.

The total power scattered into the solid angle $d\Omega$ at $\underline{R}$ is given by equation 2.28 and the spectral density function (2.26) is given by:

$$S(\underline{K},\omega') = \sum_{\mu=1}^{3} \frac{|\xi^{\mu}|^2}{\omega_{\mu}^2(\underline{K})} \quad \frac{1}{\pi} \qquad (2.37)$$

$$\times \left\{ \frac{\frac{\Gamma_{\mu}(\underline{K})}{(\omega' - [\omega_o + \omega_{\mu}(\underline{K})])^2 + \Gamma_{\mu}^2(\underline{K})} + \frac{\Gamma_{\mu}(\underline{K})}{(\omega' - [\omega_o - \omega_{\mu}(\underline{K})])^2 + \Gamma_{\mu}^2(\underline{K})}}{2 \times \sum_{\mu=1}^{3} \frac{|\xi^{\mu}|^2}{\omega_{\mu}^2(\underline{K})}} \right\}$$

It is seen from equation 2.37 that the spectrum of the scattered radiation consists in general of three pairs (μ = 1,2,3) of doublets split around the incident light frequency ω_o by the amount $\pm\ \omega_{\mu}(\underline{K})$. Also the lineshape of the Brillouin components is lorentzian with linewidth $\Gamma_{\mu}(\underline{K})$ and lifetime $2\pi/\Gamma_{\mu}(\underline{K})$.

The coefficients $|\underline{\xi}^{\mu}|$ act as weighting factors which determine the relative intensity* of each Brillouin component. The magnitude of these coefficients depend on (2.22, 2.23) propagation directions and polarizations of the phonon and photons and on the value of the photoelastic tensor components.

---

*The relation between the weighting factors and the classical scattering coefficient defined by Fabelinskii (1968) is given in Appendix B.

In the present experiment values for the weighting factors were determined from equations 2.22 and 2.23. The propagation directions and polarizations of the phonons and photons were used as parameters in these equations and the results are given in Tables I-V. Also presented in these Tables are expressions for the phonon phase velocity as a function of the elastic constants. The relation between the phase velocity and the elastic constants is discussed in the following section.

2.7 Theory of Elastic Waves in Cubic Crystals

In this section a brief description of the theory of elastic waves in cubic crystals is presented. A more complete analysis is presented in Appendix A.

The theory of Brillouin scattering presented in the previous sections of this chapter allows for a measure of the phase velocity (ω_μ/K) of the acoustic vibrations as a function of propagation direction. In the present section theoretical predictions for the magnitude and angular dependence of this velocity are considered.

The theory of lattice vibrations is well established. It is known (Fedorov, 1968) that a general formulism exists for calculating the phase velocity of acoustic vibrations. In this formulism the phase velocity is obtained

by diagonalizing the so-called dynamical matrix. It is known (Maradudin et al., 1963) that when the wavelength of the lattice vibrations become very long compared to the interatomic distances the elements of this matrix can be written in terms of the elastic constants. In this limit the phase velocity can be determined from an eigen-equation for the normal mode vibrations. This equation is referred to as Christoffel's equation and may be written:

$$\sum_{m=1}^{3} (\Lambda_{im} - V^2 \delta_{im})\ U_m = 0 \qquad \text{for } i = 1, 2, 3 \tag{2.38}$$

where the second-rank tensor Λ_{im} is given by:

$$\Lambda_{im} = \sum_{j,\ell=1}^{3} \lambda_{ij\ell m}\ (\hat{\ell}_K)_j\ (\hat{\ell}_K)_\ell \tag{2.39}$$

and $\lambda_{ij\ell m} = \dfrac{C_{ij\ell m}}{\rho}$

where $\hat{\ell}_K$ is the unit phonon wavevector with components $(\hat{\ell}_K)_\ell$ ($\ell = 1, 2, 3$) along the cube axis, $\lambda_{ij\ell m}$ the reduced elastic modulus tensor, $C_{ij\ell m}$ the elastic constant tensor, ρ the mass density, V the phase velocity and U_m the m-th component of the unit displacement vector ($\hat{U}$) of the acoustic vibration. The cube axes are chosen parallel to the four-fold rotational axes of the cubic lattice.

Christoffel's equation (2.38) is the eigen-equation for normal mode vibrations where unit polarization vectors of the phonons are the eigenvectors and the square of the phase

velocity is the eigen-value. The eigen-values are determined from the root of the characteristic equation:

$$\left|\Lambda - V^2\delta_{im}\right| = 0 \qquad (2.40)$$

The problem of determining the normal mode acoustic vibrations in an elastic solid reduces to solving for the eigen-vectors $(\hat{U})$ and eigen-values (V^2) of the tensor Λ.

The elastic constant tensor for a cubic crystal contains only three non-zero components (Nye, 1957), namely C_{11}, C_{12} and C_{44}. (Note: the reduced form of the elastic constants has been used, see Appendix A (A4)). The components of the Λ tensor (2.39) are given by:

$$\begin{aligned}
Q_{11} &= C_{11}\ell_1^2 + C_{44}(\ell_2^2 + \ell_3^2) \\
Q_{22} &= C_{44}\ell_1^2 + C_{11}\ell_2^2 + C_{44}\ell_3^2 \\
Q_{33} &= C_{44}(\ell_1^2 + \ell_2^2) + C_{11}\ell_3^2 \qquad (2.41) \\
Q_{12} &= Q_{21} = (C_{12} + C_{44})\ \ell_1\ell_2 \\
Q_{13} &= Q_{31} = (C_{12} + C_{44})\ \ell_1\ell_3 \\
Q_{23} &= Q_{32} = (C_{12} + C_{44})\ \ell_2\ell_3
\end{aligned}$$

where $Q = \rho\Lambda$ and $(\hat{\ell}_K)_j = \ell_j$.

As a sample solution to the problem of determining the normal mode vibrations in a cubic crystal consider

the following Brillouin scattering experiment. Light is incident along the edge of the cube and scattered light is observed at an angle of $\theta = 90°$ along another edge of the cube.

Let the light be incident along (100) and scattered along (010). From conservation of momentum the wavevector of the scattering vibration is given by:

$$\underline{K} = \underline{k} - \underline{k_o} = \sqrt{2}k_o \left(\frac{-1}{\sqrt{2}}, \frac{1}{\sqrt{2}}, 0\right) \qquad (2.42)$$

and the unit vector:

$$\hat{\ell}_K = \left(\frac{-1}{\sqrt{2}}, \frac{1}{\sqrt{2}}, 0\right) \qquad (2.43)$$

The components of the tensor Q (2.41) are given by:

$$\begin{aligned} Q_{11} &= Q_{22} = \frac{1}{2}(C_{11} + C_{44}) \\ Q_{33} &= C_{44} \\ Q_{12} &= Q_{21} = -\frac{1}{2}(C_{12} + C_{44}) \\ Q_{13} &= Q_{23} = 0 \end{aligned} \qquad (2.44)$$

The eigen-equation (2.38) can be written in the expanded form:

$$\begin{aligned} (Q_{11} - X)U_1 + Q_{12}U_2 &= 0 \\ Q_{12}\,U_1 + (Q_{11} - X)U_2 &= 0 \\ (Q_{33} - X)U_3 &= 0 \end{aligned} \qquad (2.45)$$

where $X = \rho V^2$ is the eigen-value for this set of equations. For a non-trivial solution the determinant of the matrix $(Q - X\delta_{im})$ must vanish (2.40):

$$\begin{vmatrix} Q_{11}-X & Q_{12} & 0 \\ Q_{12} & Q_{11}-X & 0 \\ 0 & 0 & Q_{33}-X \end{vmatrix} = 0 \qquad (2.46)$$

or

$$[(Q_{11} - X)^2 - Q_{12}^2] \, (Q_{33} - X) = 0$$

The three non-trivial solutions to the characteristic equation (2.46) are:

i) $X_1 = \rho V_1^2 = C_{44}, \quad \hat{U} = (001)$

ii) $X_2 = \rho V_2^2 = \frac{1}{2}(C_{11} - C_{12}), \; \hat{U} = \sqrt{2} \, (\frac{1}{2}, \frac{1}{2}, 0)$

which correspond to the two transverse waves ($\hat{U} \cdot \hat{\ell}_K = 0$) and

iii) $X_3 = \rho V_3^2 = \frac{1}{2}(C_{11} + C_{12} + 2C_{44})$

$$\hat{U} = \sqrt{2} \, (-\tfrac{1}{2}, \tfrac{1}{2}, 0)$$

which is a longitudinal wave ($\hat{U} \cdot \hat{\ell}_K = 1$)

In a similar manner Christoffel's equation (2.38) can be solved for any arbitrary direction of wave propagation ($\hat{\ell}_K$). The solutions provide the polarization ($\hat{U}$) and phase velocity (V) of the elastic wave. In each case the phase velocity is given as a function of the mass density (ρ) and the elastic constants ($C_{\alpha\beta}$).

Results for the polarization and phase velocity of the acoustic vibrations which are relevant to the present experiment are given in Tables I-V. Presented are the frequency shifts (cm^{-1}) calculated from the Brillouin

formula (2.2) where the phase velocity is used as a parameter. Also given are the weighting factors $\xi^{\mu}_{\sigma\tau}$ defined by equations 2.22 and 2.23 where the subscripts σ and τ refer to the polarizations of the incident and scattered radiation respectively.

TABLE I

Fine structure of light scattered in a cubic crystal for which light is incident and observed along an edge of the cube. ($\underline{k}_o = k_o(100)$, $\underline{k} = k_o(010)$, $\theta = 90°$)

Phonon † Mode μ	Frequency Shift (cm^{-1}) *	Weighting Factor $\xi^{\mu}_{\sigma\tau}$ #			
		$\xi^{\mu}_{33} = \xi^{\mu}_{\perp\perp}$	$\xi^{\mu}_{31} = \xi^{\mu}_{\perp\parallel}$	$\xi^{\mu}_{23} = \xi^{\mu}_{\parallel\perp}$	$\xi^{\mu}_{21} = \xi^{\mu}_{\parallel\parallel}$
T_1	$\sqrt{\frac{C_{11} - C_{12}}{2\rho}}$	0	0	0	0
T_2	$\sqrt{\frac{C_{44}}{\rho}}$	0	$\frac{P_{44}}{\sqrt{2}}$	$\frac{P_{44}}{\sqrt{2}}$	0
L	$\sqrt{\frac{C_{11} + C_{12} + C_{44}}{2\rho}}$	P_{12}	0	0	P_{44}

$\xi^{\mu}_{\sigma\tau}$ are the weighting factors (section 2.5, equations 2.22, 2.23) for which the polarizations of the incident and scattered radiation are denoted by the subscripts σ and τ respectively. The correspondence 1,2,3 -- x,y,z is used and the notation $\perp,\parallel$ denotes these polarizations as perpendicular or parallel to the scattering plane, respectively (x=(100), y=(010), z=(001), with respect to the cubic axes).

† The modes T_1 and T_2 are polarized parallel and perpendicular to the scattering plane, respectively.

* The common factor $\frac{\sqrt{2}n}{C\lambda}$ has been deleted in the expressions for the frequency shifts.

TABLE II

Fine structure of light scattered in cubic crystal for which light is incident and observed along a diagonal to the faces of the cube. ($\underline{k}_o = \frac{k_o}{\sqrt{2}}(\bar{1}10)$, $\underline{k} = \frac{k_o}{\sqrt{2}}(110)$, $\theta = 90°$)

Phonon † Mode μ	Frequency Shift (cm^{-1}) *	Weighting Factor $\xi^{\mu}_{\perp\perp}$	$\xi^{\mu}_{\perp\parallel}$	$\xi^{\mu}_{\parallel\perp}$	$\xi^{\mu}_{\parallel\parallel}$
T_1	$\sqrt{\frac{C_{44}}{\rho}}$	0	0	0	0
T_2	$\sqrt{\frac{C_{44}}{\rho}}$	0	$\frac{P_{44}}{\sqrt{2}}$	$\frac{P_{44}}{\sqrt{2}}$	0
L	$\sqrt{\frac{C_{11}}{\rho}}$	P_{12}	0	0	$\frac{P_{11}-P_{12}}{2}$

† The modes T_1 and T_2 are polarized parallel and perpendicular to the scattering plane, respectively.

* The common factor $\frac{\sqrt{2}n}{C\lambda}$ has been deleted in the expressions for the frequency shifts.

TABLE III

Fine structure of light scattered in a cubic crystal for which light is backscattered along an edge of the cube. ($\underline{k}_o = k_o(\bar{1}00)$; $\underline{k} = k_o(100)$, $\theta=180°$)

		Weighting Factor $\xi^{\mu}_{\sigma\tau}$	
Phonon Mode μ	Frequency Shift (cm^{-1}) *	$\xi^{\mu}_{33} = \xi^{\mu}_{22}$	$\xi^{\mu}_{32} = \xi^{\mu}_{23}$
T_1	$\sqrt{\frac{C_{44}}{\rho}}$	0	0
T_2	$\sqrt{\frac{C_{44}}{\rho}}$	0	0
L	$\sqrt{\frac{C_{11}}{\rho}}$	P_{12}	0

* The common factor $\frac{2n}{C\lambda}$ has been deleted in the expressions for the frequency shifts.

TABLE IV

Fine structure of light scattered in a cubic crystal for which light is backscattered along a diagonal to the face of the cube. ($\underline{k}_o = \frac{k_o}{\sqrt{2}}(\bar{1}\bar{1}0)$, $\underline{k} = \frac{k_o}{\sqrt{2}}(110)$, $\theta = 180°$)

Phonon † Mode μ	Frequency Shift (cm^{-1}) *	Weighting Factor $\xi^{\mu}_{\sigma\tau}$			
		ξ^{μ}_{33}	ξ^{μ}_{31} $=\xi^{\mu}_{32}$	ξ^{μ}_{13} $=\xi^{\mu}_{23}$	$\xi^{\mu}_{11}=\xi^{\mu}_{12}$ $=\xi^{\mu}_{21}=\xi^{\mu}_{22}$
T_1	$\sqrt{\frac{C_{11}-C_{12}}{2\rho}}$	0	0	0	$\frac{P_{11}-P_{12}}{4}$
T_2	$\sqrt{\frac{C_{44}}{\rho}}$	0	0	$\frac{P_{44}}{\sqrt{2}}$	0
L	$\sqrt{\frac{C_{11}+C_{12}+2C_{44}}{2\rho}}$	P_{12}	0	0	$\frac{P_{11}+P_{12}-2P_{44}}{4}$

† The transverse modes T_1 and T_2 are polarized along $(1\bar{1}0)/\sqrt{2}$ and (001), respectively.

* The common factor $\frac{2n}{C\lambda}$ has been deleted in the expressions for the frequency shifts.

TABLE V

Fine structure of light scattered in a cubic crystal for which light is incident along an edge of the cube and observed at 90° along a diagonal to the face of the cube. ($\underline{k}_o = k_o(100)$, $\underline{k} = \frac{k_o}{\sqrt{2}}(011)$)

Phonon Mode μ	ρV^2 (V, is the sound velocity) *
T_2 † (pure)	$(C_{11} - C_{12} + 2C_{44})/4$
Q.T_1 (quasi)	$(3C_{11} + 6C_{44} + C_{12})/8$
Q.L	$-\frac{1}{8} + \sqrt{(C_{11} + C_{12})^2 + 4(C_{12} + C_{44}) \cdot (-C_{11} + 4C_{12} + 5C_{44})}$

† The pure transverse T_2 mode is polarized perpendicular to the scattering plane.

* The frequency shifts are given by the Brillouin formula (2.2). The appropriate weighting factors are not given here since the quasi-nature of the vibrational modes leads to a lengthy formulation of these factors. However, it has been determined that for this scattering geometry all modes contribute to the scattered field; whether sufficient to be detected has not been determined.

CHAPTER 3

EXPERIMENTAL METHODS

3.1 Introduction

This chapter presents a description of the experimental apparatus and method used to perform the Brillouin scattering experiments. The general experimental arrangement is outlined and followed by a detailed description of the individual components.

3.2 Experimental Arrangement

A schematic of the present experimental apparatus appears in Figure 2 for both the right-angle and backscattering geometries used.

The light source was an argon-ion laser operating single mode in the 5145 Å line. The laser beam entered a light tight box which contained the sample and optics. For right-angle scattering the light was focussed onto the sample by a lens of 180 mm. focal length. The sample, mounted on a goniometer, was positioned with one of its faces normal to the incident laser beam. The sample was aligned to within ±30' by matching the specularly reflected beam from the front face of the crystal to the incident laser beam.

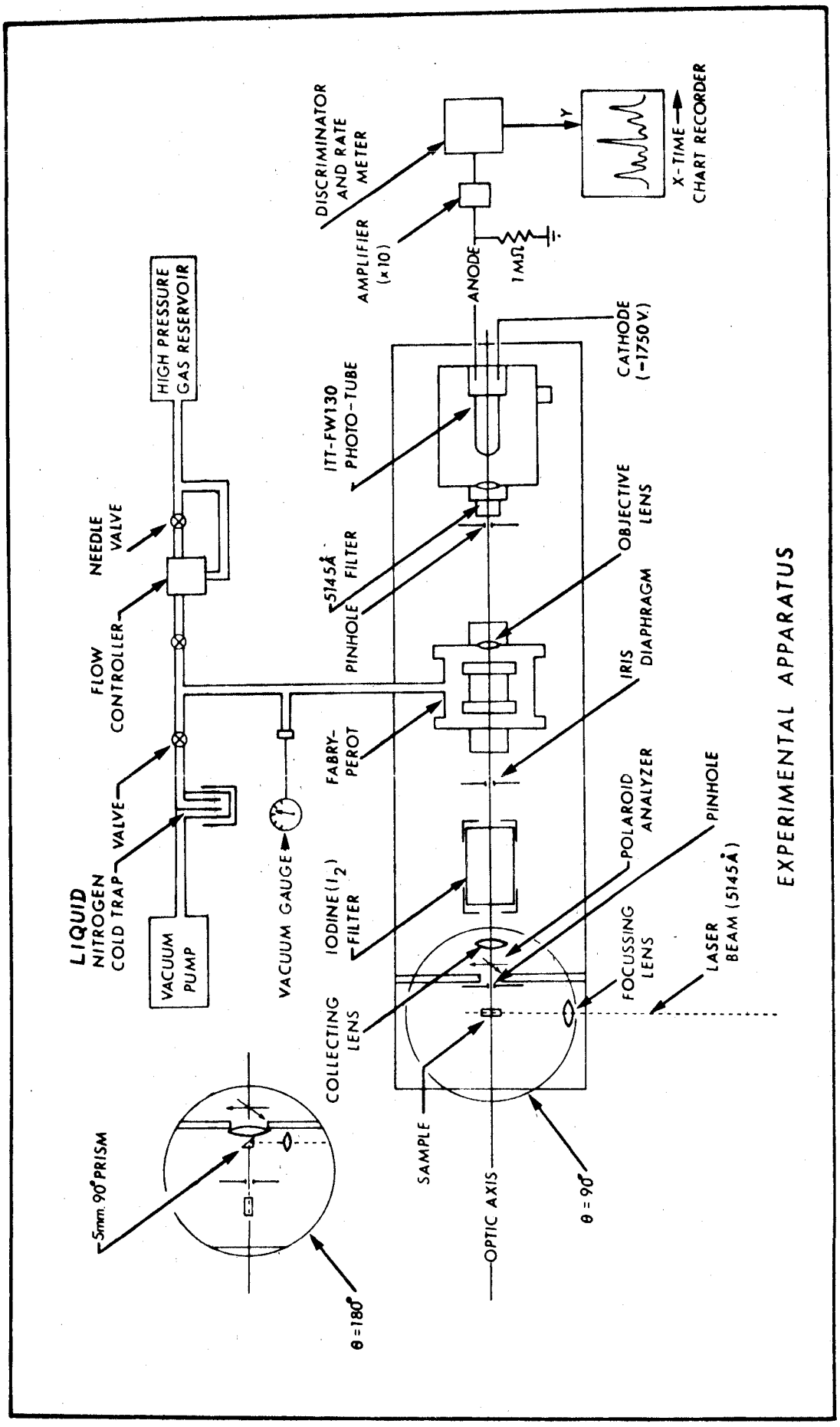

Figure 2. A schematic diagram of the experimental apparatus.

A 1mm. diameter pinhole was positioned about 15mm. from the sample, along a line at right angles to the laser beam. This pinhole served as the source aperture. A sheet polaroid could be inserted adjacent to this pinhole to investigate the polarization characteristics of the scattered light. The scattered light was collected and collimated by an achromatic lens of 115mm. focal length. The light then passed through a molecular iodine filter that attenuated the strong Rayleigh component found in the scattered light. The filtered light passed through an adjustable iris diaphragm and entered a pressure scanned Fabry-Perot interferometer.

An objective lens with a focal length of 35cm. served as the exit window of the Fabry-Perot and focussed the interference pattern onto a metal screen. A 1mm. diameter pinhole was mounted on this screen and positioned at the center of the interference pattern. Adjacent to this pinhole a 5145Å filter with 10Å bandpass was inserted to discriminate against luminescence from the sample and spectral lines from the laser plasma. Finally, the scattered light was allowed to enter a photomultiplier tube housing which contained an ITT FW-130 photomultiplier tube. The photomultiplier response was fed into a photon counting system and eventually displayed on a chart recorder.

The scattering angle (θ) was measured by a triangulation technique. The vertices of the reference triangle were located

at the sample, the center of the pinhole adjacent to the photomultiplier tube and at a reference position along a line defined by the incident laser beam. Using the cosine law and measuring the length of the sides of this triangle the scattering angle was determined.

In the backscattering geometry the laser beam was focussed by a 197mm. focal length achromatic lens through a 90° prism onto the sample. The prism was mounted in front of the 115mm. focal length achromatic collecting lens. A 7mm. diameter spot at the center of the collecting lens was made opaque to prevent collection of specularly reflected light from the front face of the crystal. An adjustable iris diaphragm was also inserted between the 90° prism and the sample to aid in the elimination of this reflected light.

A spectrum was obtained by changing the gas pressure between the Fabry-Perot plates linearly with time. The frequency output of the spectrometer was thus scanned linearly in time and one effectively obtains an output on the chart recorder of light intensity versus frequency.

Component Description

3.3. Light Source

The light source was a Spectra Physics model 165 Argon-ion laser tuned to the 5145Å line. A single mode output was

obtained by using a Spectra Physics model 589 intracavity tilted etalon, as described by Hercher (1969). Such an etalon is sufficiently detuned that it is decoupled from the main laser cavity. In such a situation it acts simply as a bandpass transmission filter.

The free spectral range of the intracavity etalon (8 GHz) is larger than the total gain bandwidth of the laser (6 GHz) and thus transmits only one mode of the laser line. Different modes can be selected by rotation of the etalon. The bandpass of the etalon was less than the separation of adjacent cavity modes (approximately 143 MHz) and thus single mode operation was obtained. The single mode power output was found to be about 50% of the total multimode power and no drift in frequency was detected within the instrumental resolution of ~1GHz.

The laser output was checked for single mode operation with the Spectra Physics model 470 Optical Spectrum Analyser. Figure 3 shows a typical oscilloscope trace for both the multimode pattern and for the single mode operation resulting from the use of the intracavity etalon.

Molecular Iodine Filter

3.4 Introduction

A major difficulty in Brillouin scattering experiments in solids is the large amount of stray light scattered at

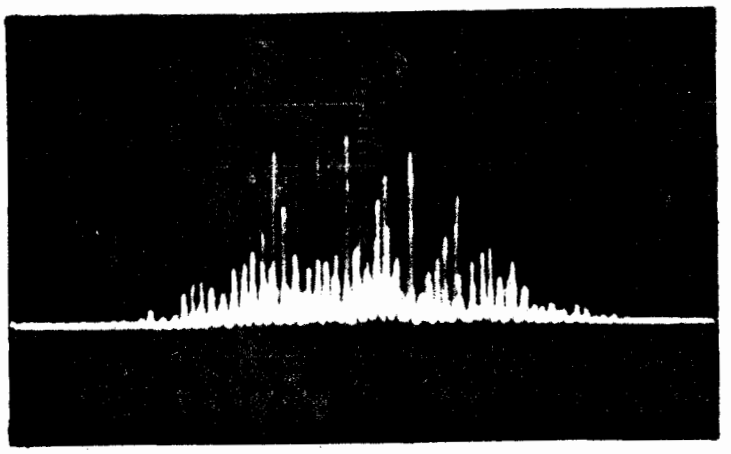

(a) Free-Running; No Intracavity Etalon (~850 MHz/cm)

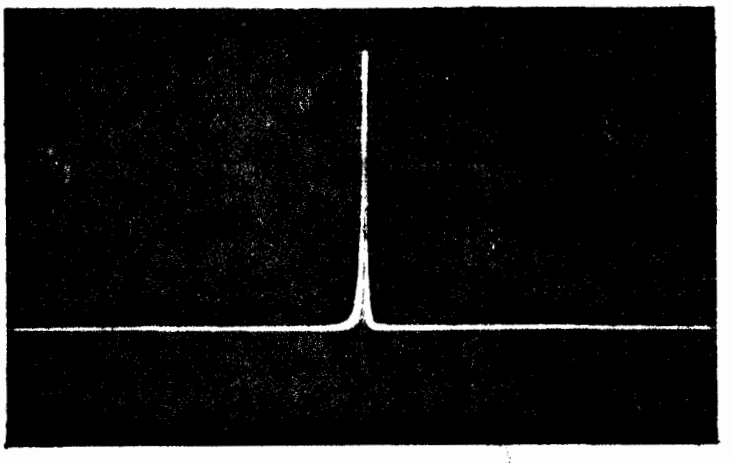

(b) Single Mode Obtained with Intracavity Etalon (~425 MHz/cm)

Figure 3. Free-running (a) and single mode (b) argon-ion laser operation at 5145 Å showing relative intensity (vertical scale) versus frequency (horizontal scale).

the unshifted laser frequency. The intensity of this Rayleigh component may be so great that its "wings" completely mask the signal under study. In the scattering experiments performed on ZnSe this was found to be the case and some method had to be found to overcome this difficulty.

The problem was resolved by using a molecular iodine (I_2) filter (Devlin et al., 1971) which has a strong absorption line situated within the gain profile of the 5145Å line of the argon-ion laser.

The specific iodine transition used is approximately 1500 MHz higher in frequency than the center of the argon-ion laser gain profile and approximately 700 MHz in width. That mode of the argon-ion laser that is closest to the center of this transition is chosen by tilting the intracavity etalon, whose operation was described in the previous section. Attenuation results from absorption in the iodine vapour and can be varied by changing the concentration of iodine vapour in the filter.

3.5 Construction

The molecular iodine filter was made from a 5-cm. diameter pyrex tubing, 10-cm. in length, whose ends were sealed with standard optically flat pyrex glass. An amount of solid iodine (I_2) was placed in the cell corresponding to approximately 40 mg/cc. of cell volume. The cell was evacuated for

about ten minutes with a mechanical pump then sealed, leaving behind about one-half of the original iodine. This procedure removes the foreign gases and also ensures that there was always some solid iodine in equilibrium with its' vapour at the highest cell temperatures used (~80°C).

To prevent condensation of the iodine vapour on the end windows it was necessary to install 3-cm. diameter apertures about 1-cm. away from these end windows. Each aperture was machined in the end of a metal cylinder which fitted over the ends of the cell. Heating tape was wrapped around the cell, the wrappings were concentrated at the ends of the cell to ensure that condensation did not occur. A copper-constantan (#30 wire) thermocouple was epoxied to the center of the cell, away from the heating tape, to monitor the cell temperature.

3.6 Calibration

The attenuation provided by the filter was strongly dependent upon the partial pressure of iodine (I_2) vapour in the cell. This pressure was controlled by varying the temperature of the cell. The present cell was calibrated by measuring the laser power transmitted through the cell as a function of the cell temperature. The results are shown in Figure 4. The attenuation is given in db as a function of cell temperature. Also shown in this figure is the attenuation as a function of cell temperature for two filters used by Devlin et al., (1971), one 4.5 cm in length, the other

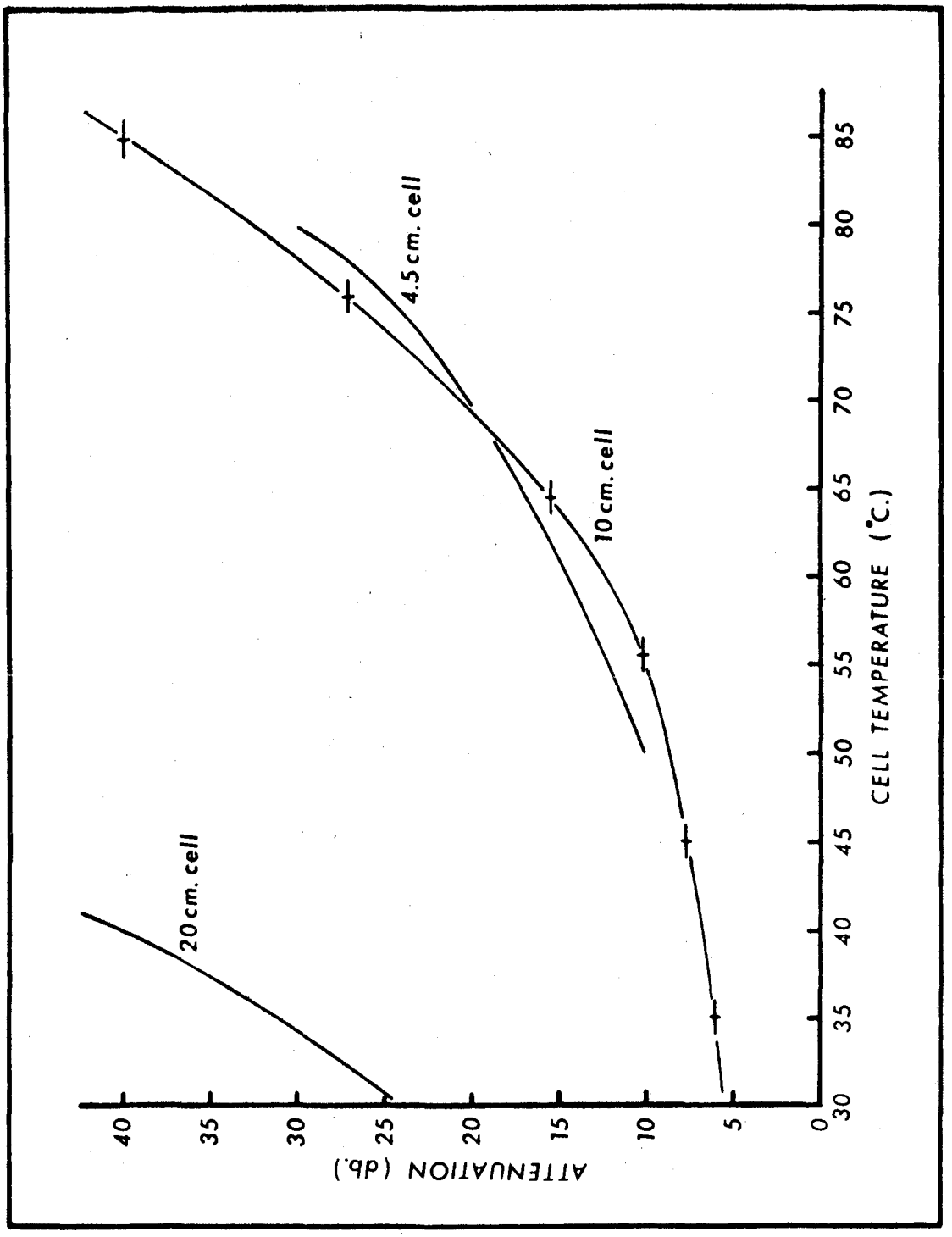

Figure 4. The attenuation of the Rayleigh line versus cell temperature for the present 10 cm long molecular iodine filter (cell) and for two filters used by Devlin et al. (1971).

20 cm. in length. In the present experiment the cell temperature was varied from about 40 to 70°C resulting in an attenuation of from 5 to 20 db.

3.7 Iodine Spectrum

The specific molecular iodine transition used has been assigned, Devlin et al.(1971), to absorption from the $\nu"=0$ level of the $X^1\Sigma_g^+$ electronic ground state to the $\nu' = 43$ vibrational level of the $B^3\pi_{ou}^+$ excited state. For the consideration of the present experiment it is important to realize that the above iodine transition is only one of many transitions occurring near (within 2 cm^{-1}) the lasing frequency. Devlin et al. (1971) mentioned that there are as many as five other sharp lines within 1 cm^{-1}. Furthermore, Kurzel and Steinfeld (1970) indicate that the following six rotational lines occur within .1Å (~.4 cm^{-1}) of the laser line:

43-0	P(12), R(14)
45-0	P(64)
49-1	R(18)
50-1	P(39)
51-1	P(53)

Kurzel et al. (1970), (from Campbell et al. (1969) and LeRoi et al., unpublished) commented that 95% of the fluorescence observed by pumping with the argon-ion laser (5145.36Å) arose from the 43'-0" transition, while only 5% was due to the 45'-0" transition. This implies that it was likely the

J = 11, 15 rotational levels of the ν' = 43 vibrational state of the $B^3\pi_{ou}^+$ that was the specific excited state which gave rise to absorption of the laser line.

The presence of these other absorption-fluorescent lines in the present experiment was evident from the observation that some of the Brillouin components were often partially or even completely attenuated. This condition proved troublesome in analyzing the data and as a consequence different scattering geometries were employed as cross-checks on each other.

This accidental overlap of an iodine absorption line with a Brillouin component is also evident in Love's (1973) Brillouin spectra of fused silica. In particular the Stokes longitudinal Brillouin component was absorbed by the filter. A thorough investigation of the iodine absorption spectrum in this region has not been carried out to date but would be valuable in that it would provide an unambiguous analysis of the observed Brillouin spectra.

Pressure Scanned Fabry-Perot Interferometer

3.8 Introduction

A pressure scanned Fabry-Perot Interferometer similar to that described by Biondi (1956) was used to frequency analyze the scattered radiation. A description of the interferometer and its operation is given in the following sections.

3.9 Construction

A cross-sectional drawing of the interferometer is shown in Figure 5. For simplicity the cross-section has been shown as symmetric about the optic axis (K). In actual fact there is only a three-fold rotational symmetry about this axis, defined by the positions of the three adjustment screws (J).

The Fabry-Perot plates (P), 98% reflecting at 5145Å, were mounted inside a cylindrically machined brass tube referred to as the plate holder (F). The plates (P) were positioned inside the plate holder by a cylindrical spacer (Q). The plates were separated from each other by a plate spacer (O). The plate spacer was formed from a set of three invar pins each of length d (0.2052 ± 0.0002 cm). The pins were mounted 120° apart in a brass ring. The dielectrically coated sufaces of the Fabry-Perot plates were held against the plate spacer by the pressure exerted from three retainer springs (I). The retainer springs acted upon a thin teflon ring which was positioned against the outer non-coated face of the plate.

The plate holder (F) was positioned inside the Fabry-Perot housing (B) by the cylindrical suspension housing (E). This assembly (E and F) was held fixed inside the Fabry-Perot housing by retainer rings (D). The ends of the Fabry-Perot housing (B) were fitted with end plates (A)

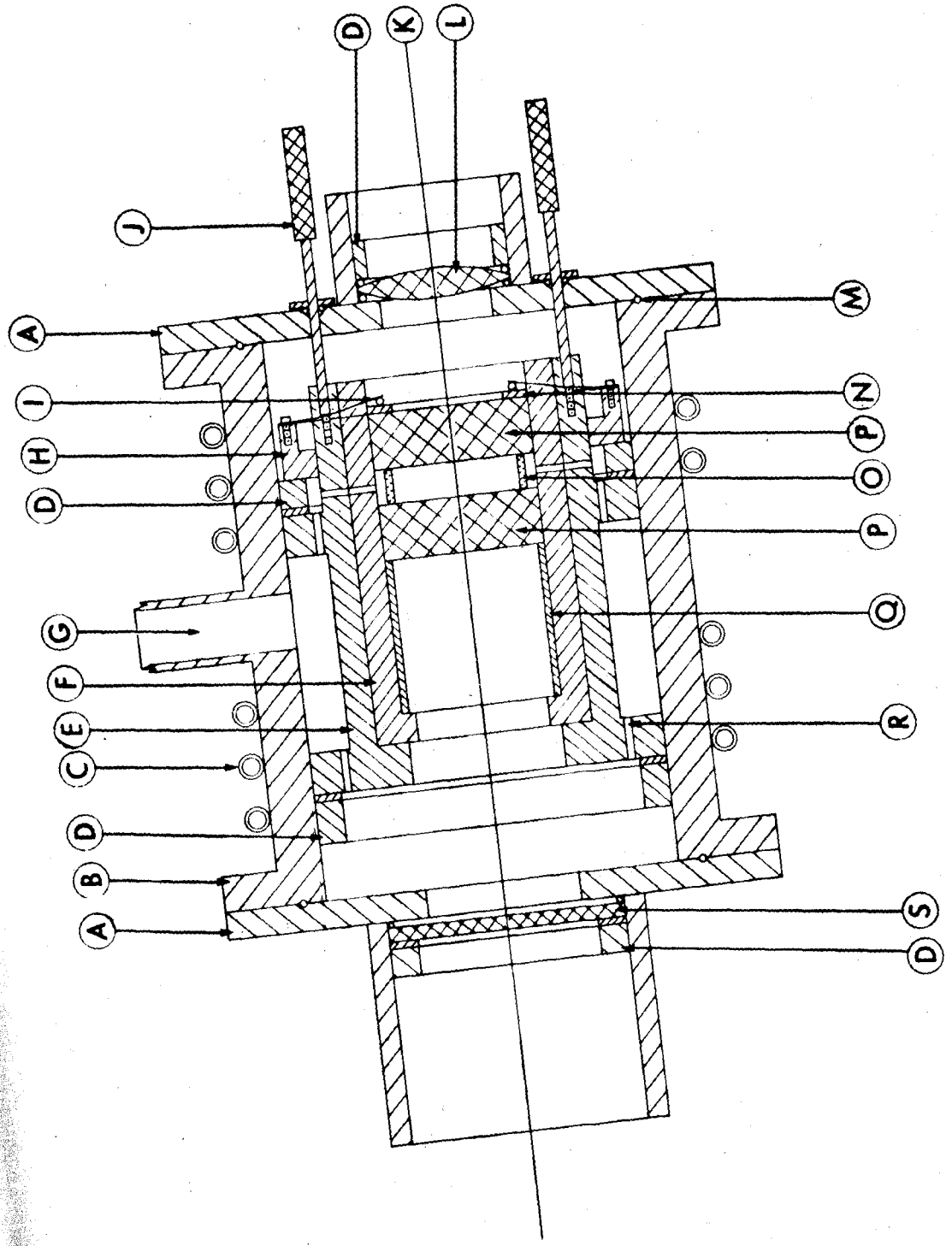

FABRY-PEROT INTERFEROMETER

Figure 5. A cross-sectional drawing of the interferometer.

Legend for Figure 5

A	End Plate
B	Fabry-Perot Housing
C	Water Cooling Coil
D	Retainer Ring
E	Cylindrical Suspension Housing
F	Plate Holder
G	Pumping Line
H	Spring Retainer Ring
I	Spring Retainer
J	Adjustment Screw
K	Optic Axis
L	Objective Lens
M	O-Ring
N	Teflon Spacer
O	Plate Spacer
P	Fabry-Perot Plate
Q	Cylindrical Spacer
R	Vent Hole
S	Glass Window

forming a vacuum seal with the o-rings (M).

A glass window (S) mounted to one of the end plates (A) served as the entrance window, allowing light to enter the housing. An achromatic lens of 35-cm. focal length, mounted on the other end plate, served as the exit window for the interferometer.

Adjustment of the Fabry-Perot plates for parallelism was accomplished by varying the pressure exerted by the three spring retainers (I) on the plates. The pressure exerted by each spring retainer was controlled by the adjustment screw (J). The interference pattern formed from a low pressure Mercury Arc Lamp was viewed and the plates aligned parallel by the standard visual procedure outlined in Jenkins and White (1957).

Vent holes (R) allowed the region between the interferometer plates as well as the rest of the interior of the housing to be pumped out and pressurized uniformly. The pumping scheme used appears in Figure 2. The housing was evacuated through the pumping line (G) and the liquid nitrogen cold trap by a mechanical vacuum pump. The cold trap was used to prevent deposit of pump oil vapour on the interferometer plates. A vacuum gauge (DVIM thermocouple) was used to monitor the gas pressure (10μ to 1000 mm. of mercury) in the interferometer.

Argon gas from a high pressure reservoir was allowed to enter the interferometer through a needle valve-constant differential flow controller assembly, as shown in Figure 2. The Moore Constant Differential Type Flow Controller (model 63BU-L) was obtained from the Moore Instrument Company Limited, Rexdale, Ontario. This flow controller maintained a linear rate of pressurization of the Fabry-Perot housing to within 1%. The rate of pressurization was controlled by the pressure of the gas reservoir (30 p.s.i.) and the needle valve setting. The desired rate of pressurization was adjusted such that the time taken to scan through one interference order was about three minutes. This rate allowed ample time to display the photomultiplier signal on a chart recorder tracing.

3.10 Operation

The scattered light was collimated by the collecting lens and allowed to enter the interferometer through the glass window (S). The Fabry-Perot interference pattern was focussed on a screen containing a pinhole aperture. The pinhole aperture was situated at the center of the pattern and thus transmitted only those wavelengths for which $2nd = m\lambda$ where n is the refractive index of the medium between the Fabry-Perot plates, d is the plate separation, and m is the order of the interference. Wavelength

(or frequency) scanning was achieved by varying the index of refraction between the plates. This was accomplished by allowing argon gas to pressurize the interferometer linearly in time.

The number of interference orders swept through in one pressurization of the Fabry-Perot housing is determined by the change in the refractive index of argon. (N.T.P. refractive index of argon is 1.000281, Biondi, 1956). The number of orders swept through in pressurizing the interferometer to atmospheric pressure is thus:

$$\Delta m = \frac{2d}{\lambda} \Delta n \cong 3$$

This corresponds to a pressure change from 10 microns to 760 millimeters of mercury for $\lambda = 5145\text{Å}$. In the present experiment the pressure changed from about 10 microns to 1,000 millimeters of mercury resulting in the display of about 4 interference orders.

The corresponding spectral range $\langle\Delta\lambda\rangle$ between orders is determined by $m\,\lambda_1 = (m-1)\,(\lambda_1 + \Delta\lambda)$. The free spectral range $\langle\Delta\lambda\rangle$ ($\langle\Delta\tilde{\nu}\rangle$) is thus given by $\langle\Delta\lambda\rangle = \frac{\lambda^2}{2d}$ ($\langle\Delta\tilde{\nu}\rangle = \frac{1}{2d}$). The free spectral range used in the present experiment was chosen to be $2.437 \pm 0.002\ \text{cm}^{-1}$ ($d=0.2052 \pm 0.0002$ cm.). With this free spectral range most of the spectra to be investigated occupied a spectral range less than $\langle\Delta\tilde{\nu}\rangle$ and thus were repeated several times (without order overlap)

as the interferometer was scanned.

3.11 Photon Counting System

An ITT FW-130 photomultiplier tube of S-20 response was used to detect the intensity of the scattered light. The photomultiplier tube was housed in a Products for Research model TE-104 refrigerated chamber. The photomultiplier tube was maintained at a temperature of -20°C ± .5°C. The cathode was maintained at a voltage of -1750 ± 10 volts with respect to the anode and the anode current passed through a 1MΩ low noise resistor. The resulting voltage signal was applied to the input of a commercial photon counting system.

The commercial counting system was obtained from the Princeton Applied Research Corporation (PAR) and consisted of a model 202 preamplifer (gain of 10), model 281 power supply and model 231 discriminator and rate meter.

The voltage signal across the 1MΩ load resistor was amplified by the preamplifier and applied to the input of the discriminator. The discriminator voltage was adjusted by displaying the rate meter output on an oscilloscope trace and adjusting the discriminator voltage (.4 volts) until the noise spikes were just eliminated. The resulting dark count was about two counts per second.

The spectra were recorded as the Fabry-Perot interferometer was linearly pressurized. The rate meter output was applied to the Y-input of a chart recorder and the tracing made as a function of time. This allowed for a recorder tracing of the intensity of the scattered radiation as a function of frequency.

3.12 Resolution

Effects on the measured linewidth of the scattered radiation will be discussed in this section. Both intrinsic and instrumental contributions will be considered.

The ultimate resolution of a Fabry-Perot Interferometer is best described in terms of its finesse. The finesse (F) is defined as the ratio of the free spectral range (FSR) of the interferometer to the spectral interval that can just be resolved by the interferometer. In this sense the spectral interval refers to the full width at half maximum intensity of an ideal monochromatic source.

In a Fabry-Perot interferometer there are three distinct contributions to this finesse. First the effect of the diameter of the pinhole used to select the central order of the interference pattern must be considered. In the present experiment this pinhole was located in front of the photomultiplier tube and in the focal plane of the interference pattern. The resolution associated with this pinhole aperture

is discussed in terms of the instrumental width. The instrumental width is defined as the fractional spread in frequency (or wavelength) at the focal plane of the interference pattern for a disc of radius R centered on this pattern. The instrumental width can be estimated from the dispersion in the interference pattern:

$$\frac{\partial R}{\partial \lambda} = \frac{f^2}{R\lambda} \ , \quad \text{(Biondi, 1956)}$$

where f is the focal length of the objective lens. The instrumental width ($\delta\nu_p$) is given by:

$$\frac{\delta\nu_p}{\nu} = \frac{\delta\lambda_p}{\lambda} \cong \frac{1}{2}\frac{R^2}{f^2} \approx 10^{-6}$$

for a 1 mm. diameter pinhole located in the focal plane of a 35-cm. focal length lens. This corresponds to an instrumental width $\delta\nu_p \cong .6$ GHz ($\delta\tilde{\nu}_p \cong .02$ cm^{-1}). The corresponding finesse is $F_p = \frac{\frac{1}{2}d}{\delta\tilde{\nu}_p} \cong 120$ • ($\frac{1}{2d} = 2.437 \pm 0.002$ cm^{-1}).

Secondly there is the contribution to the resolution from the reflectivity of the interferometer plates. The operation of the interferometer depends upon the interference between wavefronts which have undergone many reflections between the plates before being transmitted. The resolution increases with the number of such reflections and thus depends upon the reflectivity. Expressed as a finesse

(Davis, 1963) the contribution from the reflectivity of the plates, assuming no losses from the dielectric coatings, is:

$F_R = \frac{\pi\sqrt{R}}{1-R}$, where R is the reflection coefficient, assuming that both plates have the same reflectivity. In the present experiment R = .98 which corresponds to a finesse of $F_R \cong 155$. The associated instrumental linewidth is about $\delta\nu_R$ = .5 GHz. ($\delta\tilde{\nu}_R$ = 0.016 cm^{-1}).

Finally the resolution is limited by the flatness of the interferometer plates. Davis (1963) has shown that plates flat to λ/k yield a spectral finesse of about $F_D \cong k/2$. The present interferometer plates were flat to $\lambda/50$ and thus the associated flatness finesse was of the order of 25. This finesse corresponds to using the full plate area to obtain the interference pattern and can be substantially improved by using only a portion of the plates. In the present experiment the active plate area used was about 1 cm. in diameter as compared to the full plate diameter of 5 cm. Consequently an achieved experimental finesse of about 40 was not surprising. This finesse corresponds to a linewidth of about 1.8 GHz ($\sim$0.06 $cm.^{-1}$).

An instrumental contribution to the linewidth of the scattered radiation arises from the finite solid angle of observation determined by the collecting optics. This cone of light acceptance contributes to the linewidth since one

effectively samples the scattering which arises from a corresponding distribution in phonon wavevectors. To estimate the magnitude of this effect for right-angle scattering an f-number of about 15 is assumed for the collecting optics. This results in an angular spread $\delta\theta'$ about the scattering angle θ, ($\theta = 90°$) of $\delta\theta' \cong \frac{1}{2f} \approx \frac{1}{30}$ radians as viewed exterior to the crystal. The corresponding angular spread $\delta\theta$ with reference to the interior of the crystal is $\delta\theta \cong \frac{\delta\theta'}{n} \approx \frac{1}{80}$ radians ($n = 2.71$). Assuming no dispersion in the phonon phase velocity the fractional spread in frequency $\delta\nu_\theta$ can be estimated from the Brillouin formula (equation 2.2) to be:

$$\frac{\delta\nu_\theta}{\nu} = \delta\left(\frac{\theta}{2}\right) \cot\left(\frac{\theta}{2}\right) ,$$

where ν is the Brillouin frequency shift. Typically the Brillouin frequency shifts are of the order of 30 GHz ($\sim$1 cm^{-1}). The associated linewidth contribution is $\delta\nu_\theta \cong .2$ GHz (~ 0.006 cm^{-1}).

In the backscattering experiments the collecting optics are estimated to be about f/4. The associated linewidth contribution is calculated from $\frac{\delta\nu_\theta}{\nu} \cong \frac{1}{32}\left(\frac{1}{nf}\right)^3$ to be $\delta\nu_\theta \cong .7$ MHz ($\sim 10^{-5} cm^{-1}$).

Finally there is the contribution to the linewidth which arises from the frequency content of the light source.

The argon-ion laser operating single mode with a power output stable to 1% had a linewidth of about 40 MHz.

In summary the important instrumental linewidth contributions arise from the pinhole diameter and the flatness of the Fabry-Perot plates. These two contributions are comparable in magnitude and together yield an instrumental finesse of about 40, corresponding to an instrumental resolution of approximately 1 GHz. The other instrumental contributions to the apparatus width are negligible in comparison.

This apparatus width should be compared to the intrinsic phonon linewidth. As discussed in the section on Brillouin scattering the phonon can be considered as an exponentially damped fluctuation. This damped fluctuation results in broadening of the Brillouin line over that caused by the instrument (i.e. apparatus width). An estimate of the intrinsic phonon linewidth is made from Love's data (1973) and a value of about 1 GHz is obtained. This intrinsic contribution is comparable to the resolution of the present instrument (~1GHz) and thus an estimate of the phonon linewidth should be possible.

3.13 Zinc Selenide

Zinc Selenide (ZnSe) is a group II-VI semiconductor that crystallizes in the zinc-blende structure. This can be described as a two component diamond structure, or rather, two interpenetrating face-centered cubic lattices with one lattice

containing zinc atoms and the other selenium atoms. The cube sides are of length 2a and the two sublattices are displaced from each other a distance $\sqrt{3}\,\frac{a}{2}$ along the body diagonal. This structure is illustrated in Figure 6.

The symmetry of the zinc-blende structure is described in the Schönflies group notation as T_d (Nye, 1957). The elastic constant tensor for such a structure has cubic symmetry, there being only three independent elastic constants, namely C_{11}, C_{12} and C_{44}.

The two single-crystal samples used here were obtained from a large polycrystalline sample grown by the Harshaw Chemical Company. The impurity concentrations of the polycrystal were not given, however, the sample was purchased as an undoped "pure" sample. The samples were light yellow in colour and were both approximately 1 mm × 2 mm × 3 mm in size.

The density of ZnSe was taken from Lee (1970) to be 5.264 g/cc. at a temperature of 22°C and at atmospheric pressure. The refractive index at 5145Å was calculated from the results of Marple (1964). Marple using the prism refraction method fitted his results to the standard formula:

$$n^2 = A + \left[\frac{B\lambda^2}{(\lambda^2 - C^2)}\right],$$

where n is the refractive index and λ the wavelength in

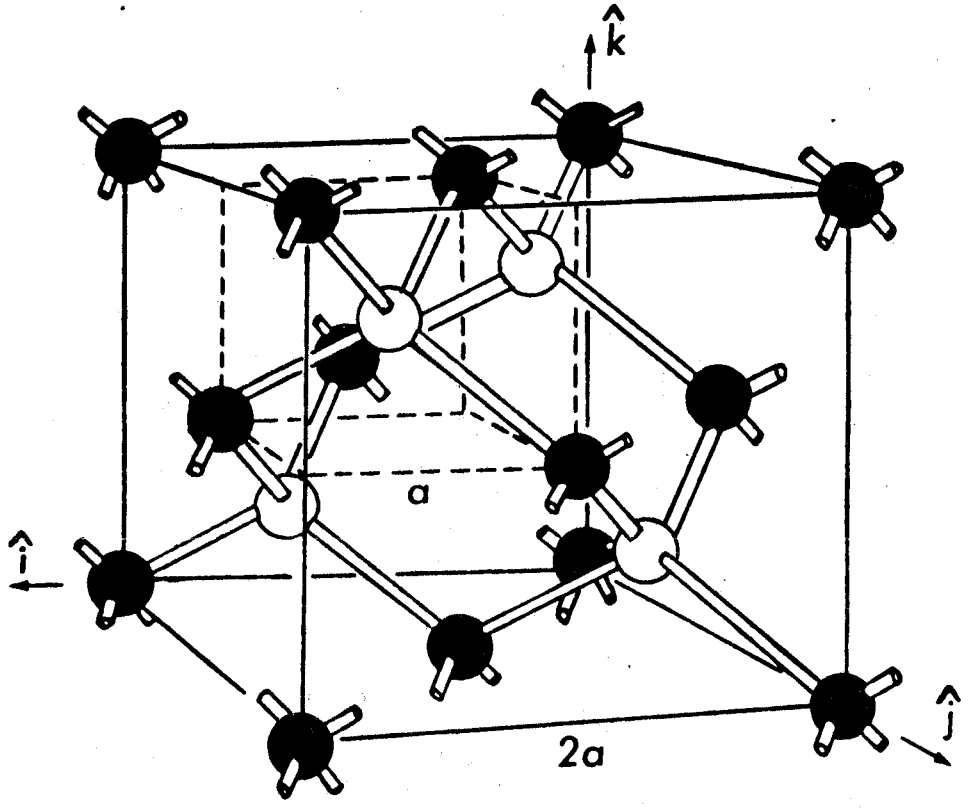

Figure 6. The zinc-blende lattice structure.

microns. For ZnSe the best values for the parameters are: $A = 4.00$, $B = 1.90$ and $C^2 = 0.113$. The refractive index calculated from the above formula is 2.705 ± 0.005 at 5145 Å. (The error of .005 is associated with the range of Marple's data).

A similar result for the refractive index results from an extrapolation of Rambauske's data (1964). Rambauske used the method of minimum deviation for a prismatic cut crystal. The extrapolated result is $2.71 \pm .01$ at 5145 Å. A value of 2.71 for the refractive index was used in the present experiment.

Two differently cut single-crystals were used in the present work and their orientations are described with respect to the laboratory reference frame in the following manner. A rectangular X, Y, Z laboratory coordinate system was adopted. The crystal designated (100) was oriented with <100> directions parallel to each of the X, Y, Z axes with faces cut and polished perpendicular to these axes. The second crystal designated (110) had <110> axes along X and Y and a <100> axis along Z with faces cut and polished perpendicular to these axes. Both crystals were X-ray oriented to better than 1° in all directions.

Standard notation, A(BC)D, (Damen et al., 1966) was used in each of the spectra. The first and last letters specify the direction of propagation of the incident and scattered

light respectively. The second and third bracketed letters specify the polarization directions of the incident and scattered light respectively. A complete description of the scattering geometry includes the particular crystal sample used. For example the notation:

$$\text{ZnSe (100)}$$
$$X(Z,\overset{Z}{\underset{X}{}})Y$$

indicates light scattering from the (100) crystal sample where the scattered light, observed at 90° from that of the incident light direction, was observed in the absence of an analyzer.

CHAPTER 4

RESULTS

4.1 Introduction

In this chapter the Brillouin spectra are analyzed and the Brillouin frequency shifts are determined. The theory of elastic waves in cubic crystals (section 2.7) and the Brillouin formula (equation 2.2) are then used to determine values for the elastic constants from these measured frequencies. In the first part of this chapter the elastic constants C_{33} and C_{44} of alpha-Quartz are determined in order to test the applicability and reliability of the experimental technique . In the second part the Brillouin spectra obtained for Zinc Selenide are presented and analyzed to provide values for the elastic constants.

4.2 Alpha-Quartz

As an evaluation of the present experimental technique several Brillouin spectra of α-Quartz were recorded. A typical spectrum is shown in Figure 7 where scattering from two transverse (T_1, T_2) and a longitudinal (L) mode is evident. (R denotes the Rayleigh component). This spectrum was not used in the present analysis because piezoelectric corrections to the elastic constants are required.

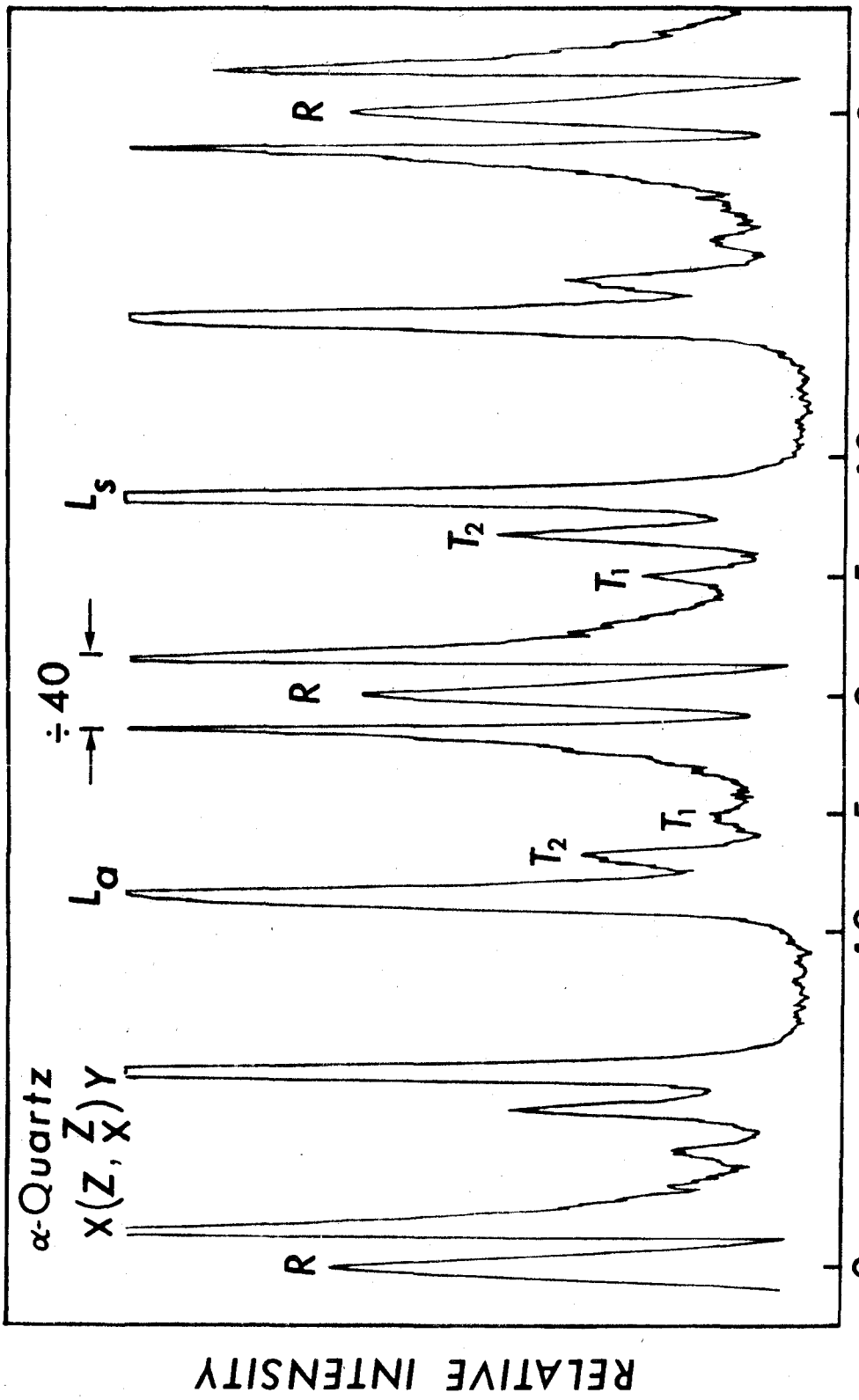

Figure 7. The Brillouin spectrum of an α-Quartz crystal with $X(Z,{}^{Z}_{X})Y$ polarization taken at 5145 Å (800 mw.) for a scattering angle $\theta = 90° 38' \pm 10'$. (s and a refer to Stokes and anti-Stokes components, respectively).

The measurements were performed on a single crystal sample obtained from the Valpey-Fisher Corporation. The crystal was a z-cut wafer which measured 2mm × 1cm × 1cm in size with the c-axis normal to the large face. The crystal was mounted with the c-axis parallel to the laboratory Z-axis and one of the three a-axes parallel to X (IRE Standards on Piezoelectric Crystals, 1949).

The density of α-Quartz is 2.6485 g/cc at 25°C (McSkimin, 1962). The refractive index was obtained from an extrapolation of Martens' (1901) data at 23°C (American Institute of Physics Handbook). The extrapolated values are : n_o = 1.548 and n_e = 1.557 at 5145 Å.

Experimentally it was found that the intensity of the Rayleigh component was comparable to that of the Brillouin components and as a result the molecular iodine filter was not required to attenuate this component. It is emphasized that this Rayleigh component was mainly due to the scattering from crystal defects and also from surface scattering.

The elastic constants C_{33} and C_{44} were determined from the measured Brillouin frequency shifts for the back-scattering geometry $\bar{Z}(Y,{}^{Y}_{X})Z$ and the results are given in Table VI. The elastic constants were determined from the sound velocities of the longitudinal ($V_L = \sqrt{\frac{C_{33}}{\rho}}$) and transverse ($V_T = \sqrt{\frac{C_{44}}{\rho}}$) phonon modes. ($\rho$ is the density of α-Quartz). The sound velocities were determined from the measured frequency shifts by using the Brillouin formula (eqn. 2.2). No corrections have been made in the present considerations for piezoelectric effects on the measured sound velocities. A discussion of the justification of this omission is presented in the Appendix, section C.

As a comparison some previously determined values for these elastic constants are also given in Table VI. It is evident that the present values for the elastic constants C_{33} and C_{44} agree to within about 2% with these previous measurements. In particular there is good agreement (.7%) between the present value of C_{44} and the Brillouin measurement of Cecchi et al. (1970). Agreement to within 2% between the present data and the previous results is in line with the expected order of agreement. The major experimental sources of error contribute an uncertainty in the measurements which are of the order of 1%. These sources of error include the degree to which the rate of pressurization of the interferometer was linear in time

TABLE VI

The Elastic Constants C_{33} and C_{44} of α-Quartz

a. Present Data

Scattering Geometry	Phonon Mode	Frequency Shift (cm^{-1})	Sound Velocity (10^5cm/sec.)	Elastic Constant (10^{10} dyn/cm^2 at 22°C)
$\bar{Z}(Y,X)Z$	T	.933±.005	4.65±.02 †	C_{44}=57.3±.5*
$\bar{Z}(Y,Y)Z$	L	1.270±.003	6.33±.01 †	C_{33}=106.1±.3*

* Indicated error limits refer to standard deviation of results and do not indicate absolute accuracy.

b. Previous Data

Reference	Method	Elastic Constant (10^{10}dyn/cm^2) C_{44}	C_{33}
1. Atanasoff et al. (1941)#	piezo-resonance (35°C)	57.86	106.8
2. Koga et al. (1958)	piezo-resonance (20°C)	58.2567 ±.0065	105.94 ±.12
3. McSkimin (1962)	ultrasonic (25°C)	58.18 ±.06	105.74 ±.10
4. Cecchi et al. (1970)	Brillouin (4880 Å , 25°C)	57.7 ±.3	105.1 ±.5

Results as corrected by Lawson's method (1941).

† Sound velocities were determined using the ordinary index of refraction (n_o).

(1%) and the error in the scattering angle (1%). Consequently, it is not surprising that the present results, which include an intrinsic error of about 1-2%, deviate within this range from the earlier measurements. In conclusion it is felt that the present results for α-Quartz confirm the correctness of the present experimental technique.

4.3 Zinc Selenide

A general description of the Brillouin spectra obtained from the single-crystal ZnSe samples is presented here. As mentioned previously (section 3.7) the accidental coincidence of an iodine absorption line with a particular Brillouin component could cause the component to be absent or severely attenuated. This problem necessitated the use of several scattering geometries so that a determination of all three elastic constants could be made. The frequency shifts were measured only for those Brillouin components which were unattenuated and symmetric. A qualitative description of the individual Brillouin spectra taken is given in the following paragraphs.

ZnSe (100) $X(Z,\frac{Z}{X})Y$ (Figure 8)

As outlined in section 3.13 this spectrum of Figure 8 was obtained using the (100) crystal with the laser beam incident along (100), polarized along (001) and the scattered

light observed along (010) in the absence of an analyzer. The scattering angle was measured to be $\theta = 91°28' \pm 16'$. The central Rayleigh component of the spectrum was chosen to be the origin of the frequency scale (cm^{-1}). A free spectral range of $\langle \Delta\tilde{\nu} \rangle = 2.437 \pm 0.002\ cm^{-1}$ was chosen for all measurements in the present experiment.

The polarization selection rules (section 2.7, Table I) predict for this orientation that light should be scattered from only two acoustic phonons. The scattering should occur from the fast transverse (T_2) and the longitudinal (L) modes. The observation of only two Brillouin components in this spectrum agrees with these predictions. The frequency shifts were measured for only the Stokes transverse (T_{2S}) component since the other modes were attenuated by the molecular iodine filter.

ZnSe (110) $X(Z,\frac{Z}{X})Y$ (Figure 9)

The polarization selection rules (section 2.7, Table II) predict scattering from the fast transverse (T_2) and the longitudinal (L) modes and these two modes can be observed in the spectrum shown in Figure 9. Attenuation of the anti-Stokes modes for both the fast transverse and longitudinal modes and the increased noise level at the estimated positions of these components is evident. The Brillouin frequency shifts were measured from the Stokes components. The

scattering angle was measured to be $\theta = 91°28' \pm 16'$.

ZnSe (100) $\bar{X}(Z, \begin{smallmatrix} Z \\ Y \end{smallmatrix})X$ (Figure 10).

In this backscattering geometry of Figure 10 the polarization selection rules (section 2.7, Table III) predict scattering from only the longitudinal mode. The Brillouin frequency shift of this mode being more than one-half of the free spectral range of the interferometer resulted in an overlap of the Stokes and anti-Stokes components. The presence of a small peak about .43 cm^{-1} on the high frequency side of the Rayleigh line is attributed to fluorescence from the iodine filter. This peak is also evident in the spectra of Figures 8, 9, 11, and 12.

ZnSe (110) $\bar{X}(Y, \begin{smallmatrix} Y \\ Z \end{smallmatrix})X$ (Figure 11)

For this geometry the selection rules (section 2.7, Table IV) predict scattering from all three phonon modes (T_1, T_2, L). However the frequency shifts of the transverse modes are such that these components (T_1 and T_2) occur near the sides of the strong longitudinal components and in the present experiment could not be resolved. Their presence was evidenced only by the increased noise level on the sides of these longitudinal components. Only the frequency shift of the Stokes longitudinal component was measured due to the slight attenuation of the anti-Stokes longitudinal

mode by the iodine filter. Also, as in Figure 10, the Stokes and anti-Stokes longitudinal components overlap.

ZnSe (110) $X(Y, \overset{Y}{X})Z$ (Figure 12)

For this scattering geometry selection rules (section 2.7 , Table V) predict that scattering should occur from a slow quasi-transverse mode ($Q.T_1$), a fast pure transverse mode (T_2) and a quasi-longitudinal mode ($Q.L$). Only the quasi-modes were observed due to the weaker scattering from the pure transverse mode. Attenuation of the Stokes quasi-longitudinal and the absence of the anti-Stokes quasi-transverse modes indicate extensive attenuation by the iodine filter. The scattering angle was measured to be $\theta = 90°48' \pm 10'$.

A summary of the measured Brillouin frequency shifts is given in Table VII. For near right-angle scattering geometries the measured frequency shifts have been corrected to correspond to 90° scattering angle. From the frequency shifts the phonon phase velocities were calculated using the Brillouin formula (equation 2.2) and the elastic constants were related to the phase velocity and scattering geometry using the procedure outlined in section 2.7 (Tables I-V).

The final values for the elastic constants were determined from a weighted average of the results which appear in Table VII. The values obtained are:

TABLE VII

Brillouin Measurements in ZnSe

Crystal Sample	Scattering Geometry	Phonon Mode	Frequency Shift (cm^{-1}) †	Result $(10^{10} dyn/cm^2)$
(100)	X(Z,X)Y	T_2	.68±.01 .680±.007	C_{44}=39.5±1.1 "=39.5±0.8
	$\bar{X}$(Z,Z)X	L	1.43±.01	C_{11}=87.2±1.3
(110)	X(Z,X)Y	T_2	.68±.01 .677±.005	C_{44}=39.5±1.1 "=38.9±0.6
	X(Z,Z)Y	L	1.014±.005 1.006±.007	C_{11}=87.6±0.8 "=86.3±1.3
	$\bar{X}$(Y,Y)X	L	1.596±.005 1.601±.005	C_{12}=51.4±1.3# "=53.4±1.3#
	$X(Y,\frac{Y}{X})Z$	Q.T_1	.51±.01	C_{12}=53.3±2.5#
		Q.L	1.160±.007 1.167±.005	C_{12}=54.0±3.5#

Indicated error limits refer to standard deviation of results and do not indicate absolute accuracy.

The results for C_{12} were determined using the final values for C_{11} and C_{44} (Table VIII)

† The listing of more than one measurement for a given scattering geometry and phonon mode indicates that these measurements were made from data which were taken on different experimental runs.

$C_{11} = 87.2 \pm 0.6$

$C_{12} = 52.4 \pm 0.8$

$C_{44} = 39.2 \pm 0.4$

in units of $10^{10} dyn/cm^2$.

Throughout the present analysis the piezoelectric nature of ZnSe has been neglected. The effect of piezoelectricity on the values determined for the elastic constants is discussed in Appendix C.

An estimate of the intrinsic phonon linewidth can be made from the present data. The experimental finesse was approximately 40 and from a measure of the increased linewidth broadening of the Brillouin components the intrinsic phonon linewidth is estimated to be about $\lesssim .1$ GHz. This value is of the order of that estimated from Love's data (~1GHz; section 3.12).

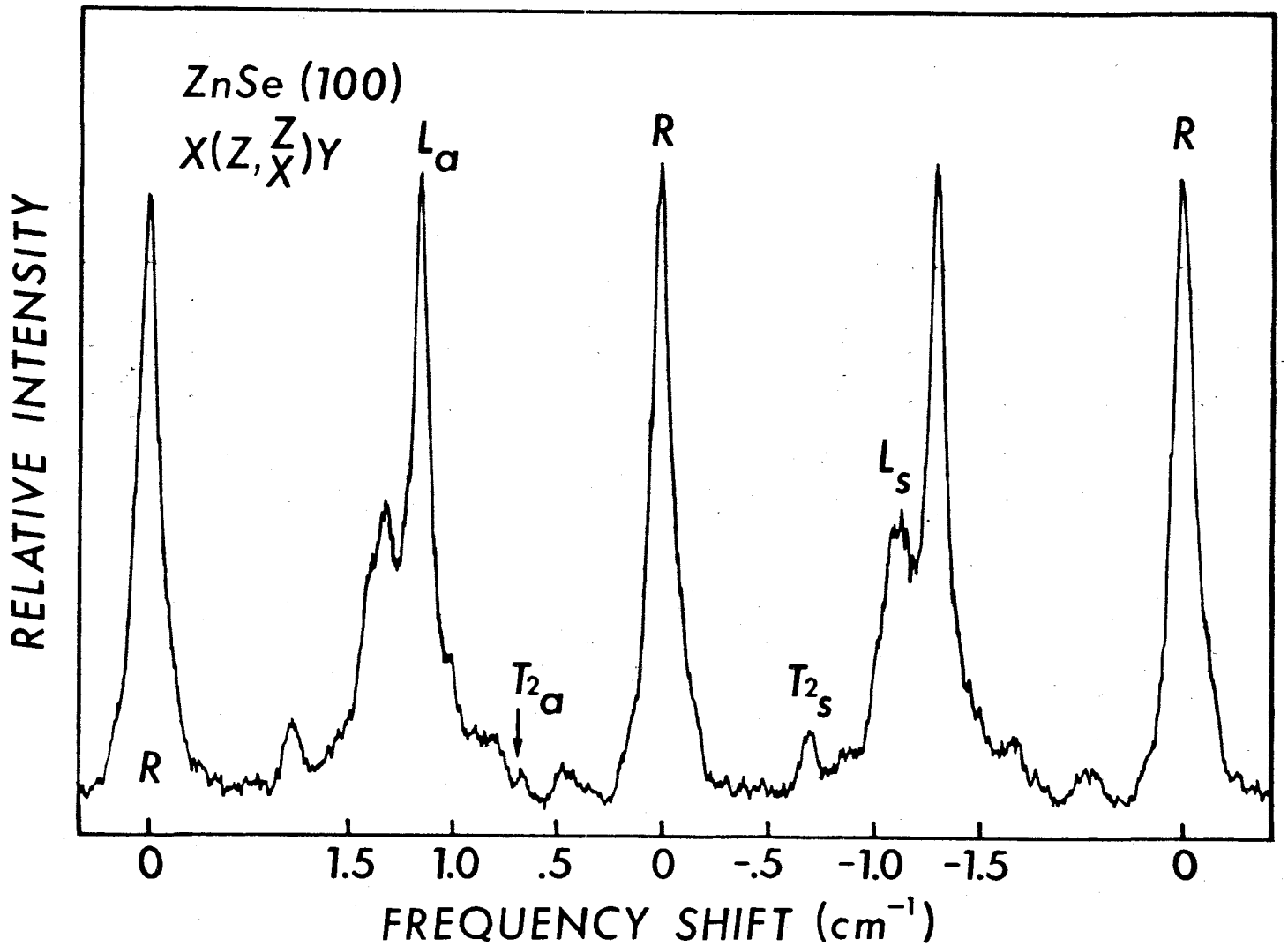

Figure 8. The Brillouin spectrum of a ZnSe (100) crystal with $X(Z,\frac{Z}{X})Y$ polarization taken at 5145 Å (950 mw.). Attenuation of the Rayleigh line was ~9db.

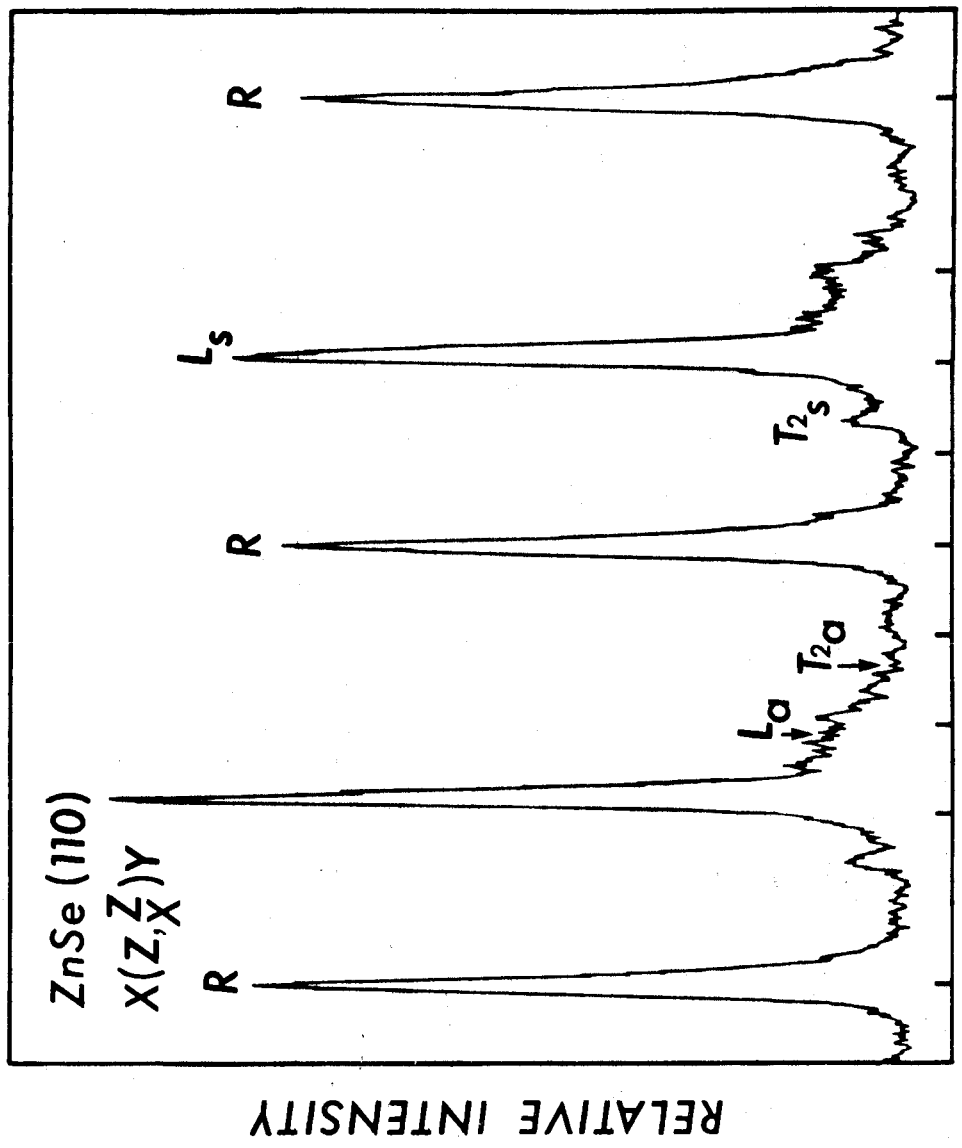

Figure 9. The Brillouin spectrum of a ZnSe (110) crystal with $X(Z,{}^{Z}_{X})Y$ polarization taken at 5145 Å (500 mw.). Attenuation of the Rayleigh line was ~10db.

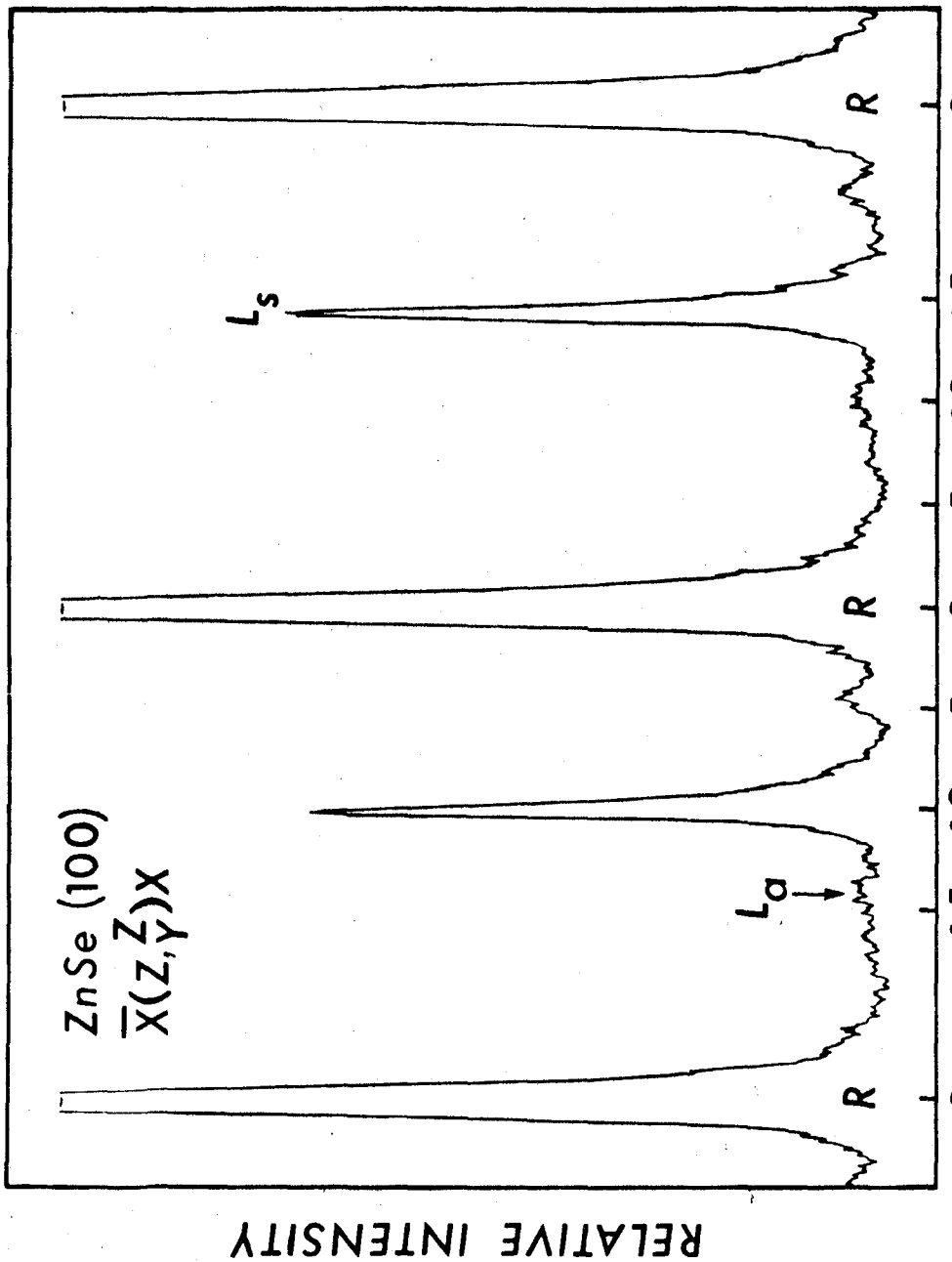

Figure 10. The Brillouin spectrum of a ZnSe (100) crystal with $\bar{X}(Z,\frac{Z}{Y})X$ polarization taken at 5145 Å (150 mw.). Attenuation of the Rayleigh line was ~11db.

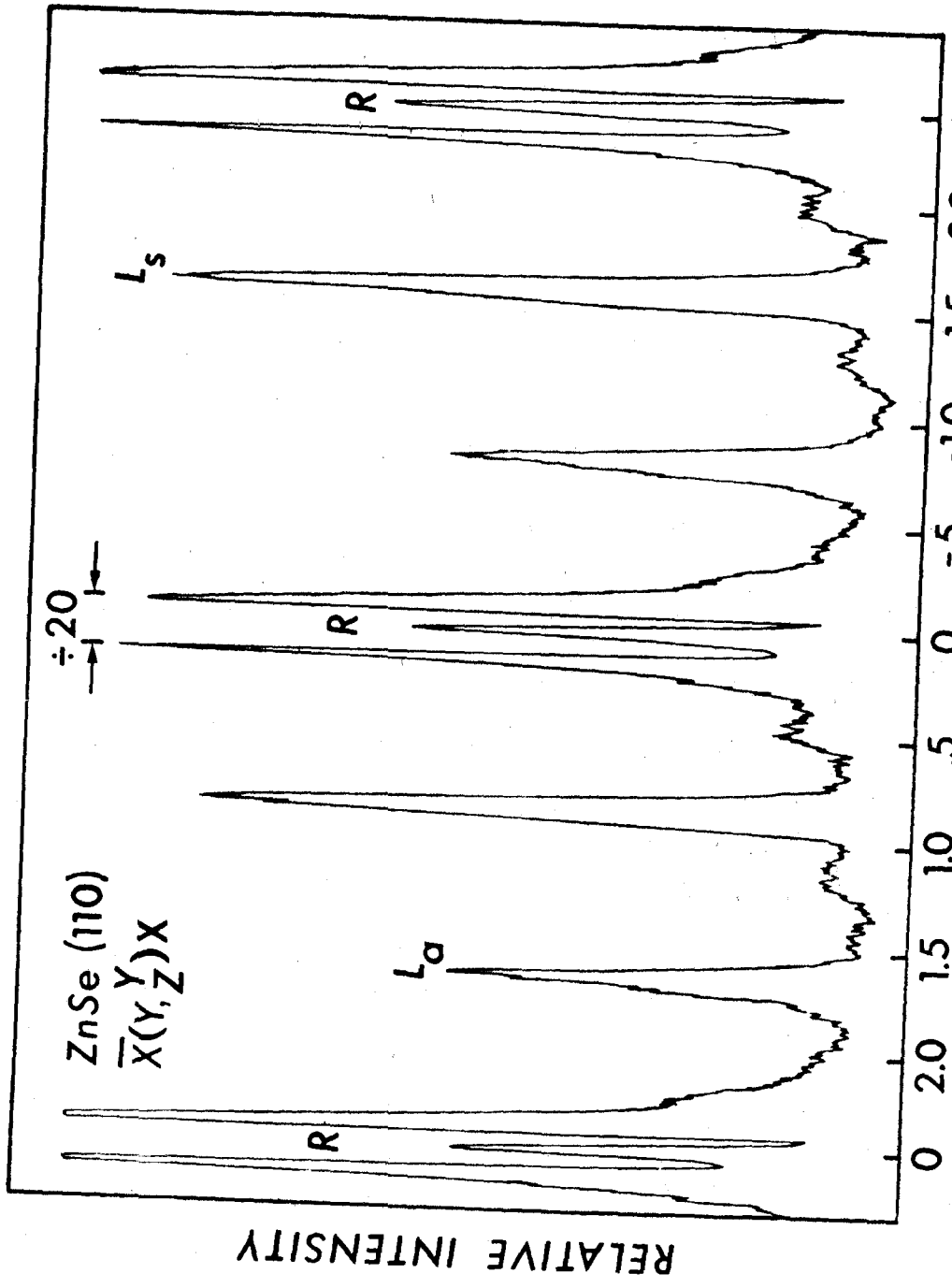

Figure 11. The Brillouin spectrum of a ZnSe (110) crystal with $\bar{X}(Y,Z)X$ polarization taken at 5145 Å (210 mw.). Attenuation of the Rayleigh line was ~16db.

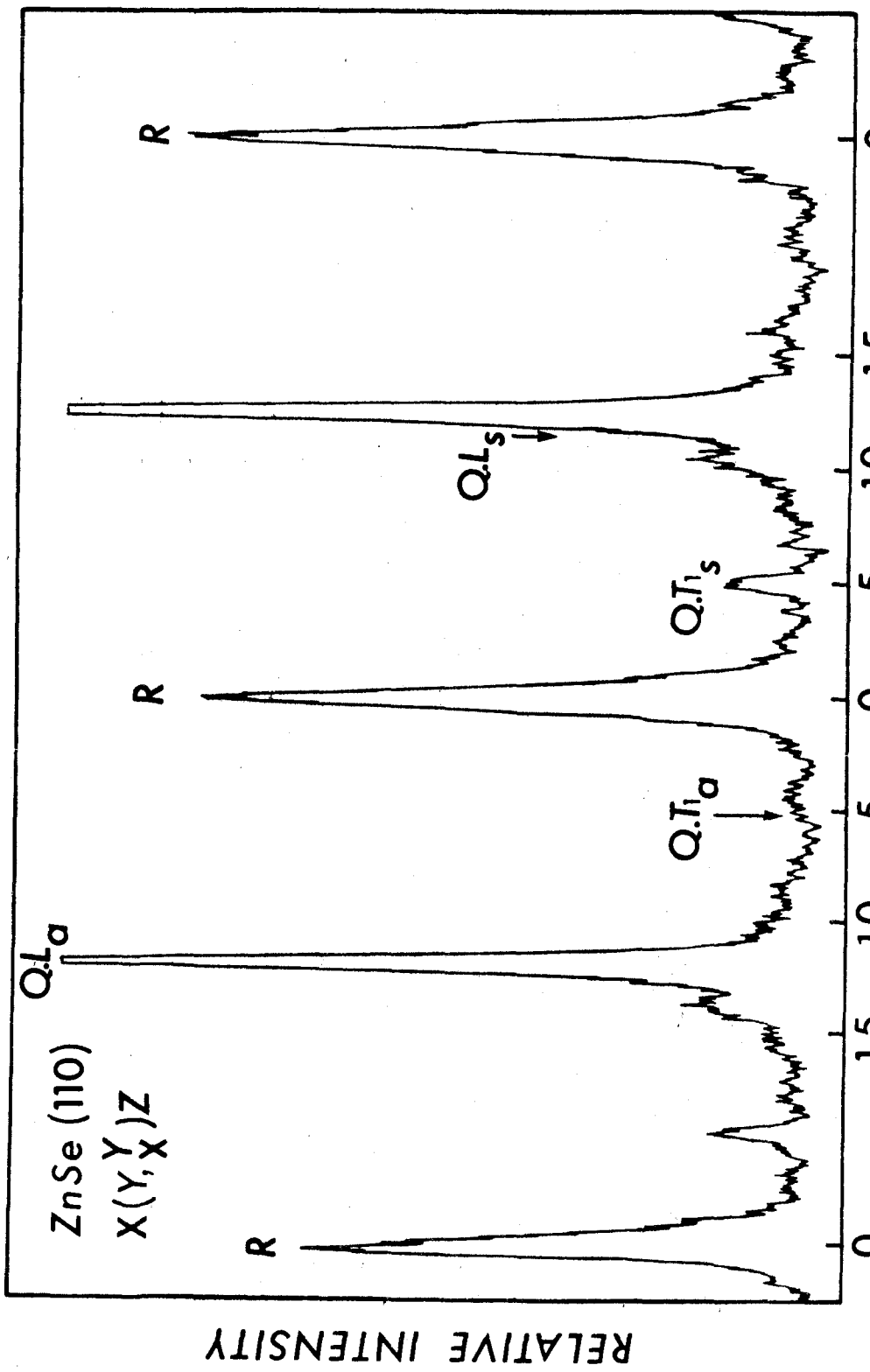

Figure 12. The Brillouin spectrum of a ZnSe (110) crystal with $X(Y, {}^{Y}_{X})Z$ polarization taken at 5145 Å (420 mw.). Attenuation of the Rayleigh line was ~9db.

CHAPTER 5

DISCUSSION

5.1 Introduction

In this chapter the results described in the previous chapter are compared to earlier measurements. In section 5.2 the values obtained for the elastic moduli of ZnSe are compared with values determined previously by Berlincourt et al. (1963) and Lee (1970) from measurements on single-crystals. In addition, the polycrystalline elastic moduli are calculated from the single-crystal values and compared in section 5.3 to the experimental values of Chung and Buessem (1967). Further, in section 5.4 an estimate of the relative magnitude of the photoelastic coefficients is made from the present data. In section 5.5 a relation between the single-crystal elastic moduli due to Martin (1970) is used to compare the present data with the earlier measurements. The chapter concludes with a comparison of the present results with those obtained from neutron data.

5.2 Single-Crystal Elastic Moduli

The present single-crystal elastic moduli of ZnSe are tabulated in Table VIII together with the previous values of Berlincourt et al.(1963) and Lee (1970). Berlincourt et al. (1963) determined the elastic constants

TABLE VIII

Elastic Constants of ZnSe

a. Elastic Constants

Elastic constants (10^{10}dyn/cm^2)	Present Work 5.264 g/cc. (295°K) 1-50 GHz Brillouin	Lee (1970) 5.264 g/cc. (295°K) 15MHz Ultrasonic	Berlincourt et al. 5.262 g/cc.(1963) (298°K) .1∿100 MHz Piezo-Resonance
C_{11}	87.2±0.6 *	85.9±0.3	81.0±6.0
C_{12}	52.4±0.8 *	50.6±0.4	48.8±6.0
C_{44}	39.2±0.4 *	40.6±0.2	44.1±1.3

b. Sound Velocities

Designation	Mode	Propagation direction	Displacement direction	Velocity (10^5cm/sec.) Lee	Present
V_1	Long	001	001	4.0386 #	4.07±.01*
V_2	Shear	001	110	2.7770 #	2.73±.01*
V_3	Long	110	110	4.5496 #	4.55±.02*
V_4	Shear	110	001	2.7782 #	2.73±.01*
V_5	Shear	110	$1\bar{1}0$	1.8323 #	1.82±.02*

* Indicated error limits refer to standard deviation of results and do not indicate absolute accuracy.

\# Lee's values accurate to .2%.

c. Anisotropy Factor (A)

$A=\frac{2C_{44}}{(C_{11}-C_{12})}$:	Present Work	Lee	Berlincourt
	2.25±.06	2.30	2.74

(25°C) from piezo-resonance measurements. In their experiment Berlincourt et al. investigated phonons with frequencies between about 100KHz and a few MHZ. Berlincourt commented that the large errors in their elastic constants resulted from the method of deriving all moduli from only one crystal plate. More recently, Lee (1970) determined the elastic moduli (22°C) using ultrasonic pulse-echo methods (McSkimin, 1961) to excite 15 MHz phonons. The discrepancy between these two sets of data was considerably in excess of the quoted experimental errors.

It is evident from Table VIII that there is agreement between our present elastic moduli and the previous results of Lee. This agreement is further evident from a comparison of the measured sound velocities shown in Table VIII. There is agreement to better than 2% between Lee's and the present measured sound velocities. However, there is a discrepancy between the present data and Berlincourt's. This discrepancy is particularly evident in the case of C_{44} where our value is about 11% smaller than Berlincourt's. Also our values of C_{11} and C_{12} are about 8% and 7% respectively, larger than Berlincourt's.

This discrepancy is further evident from a comparison of the anistropy factor ($A = 2C_{44}/(C_{11}-C_{12})$). This factor is a measure of the degree of anisotropy of the crystal. For an isotropic crystal the anisotropy factor takes on

the value 1. The anisotropy factor is calculated from the elastic constants and the results appear in Table VIII.

Due to the agreement between our results and those of Lee and the present discrepancy when compared to Berlincourt's results it is concluded that our results substantiate the correctness of Lee's work.

5.3 Polycrystalline Elastic Moduli

The only other measurement of the elastic moduli of ZnSe were carried out on polycrystalline samples by Chung and Buessem (1967). In their experiment a modified Förster-type resonance method in the kilocycle range (Spinner and Tefft, 1961) and ultrasonic methods (McSkimin, 1964) were used. The isotropic shear modulus (G*), longitudinal modulus (L) and Young's modulus (E) for a bar-shaped polycrystal were determined.

The single-crystal elastic moduli can be compared with those of the polycrystal by means of the Voigt-Reuss-Hill (V-R-H) approximation methods (Chung et al., 1967). The V-R-H approximations provide a useful scheme by which anisotropic single-crystal elastic constants can be used to estimate the isotropic polycrystalline elastic moduli. These approximations are valid for all crystal classes and can provide a practical and accurate (to better than 1%, Anderson, 1963) estimate of the mean sound velocity in

crystals.

The isotropic V-R-H moduli can be calculated from those of the single-crystal according to the following relations:

- the Bulk modulus, $K_{VRH} = K_V = K_R = K^* = C_{11} - 2C/3$
- the Shear modulus, $G_{VRH} = G^* = (G_V + G_R)/2$

where $C = (C_{11} - C_{12})$ and the subscripts V and R denote the Voigt and Reuss limiting moduli, respectively and

$$G_V = (C + 3C_{44})/5$$

and

$$G_R = 5CC_{44}/(4C_{44} + 3C).$$

Young's modulus (E) can be calculated (Anderson, 1963) from the Bulk modulus (K*) and Shear moduli (G_V and G_R) according to:

$$E = (E_V + E_R)/2 \quad \text{where}$$

$$E_i = 9\ K_i\ G_i/(3K_i + G_i) \quad \text{for } i \in \{V,R\}.$$

The V-R-H moduli are calculated from the single-crystal values according to the previous relations and the results are given in Table IX. It is evident that the V-R-H moduli calculated from both the present single-crystal moduli and those of Lee show better agreement to the experimental values of Chung et al., than do those determined from Berlincourt's data. This result is expected due to the smaller value in the anisotropy factor for both the present samples and those of Lee as compared to that

TABLE IX

The Isotropic Polycrystalline Elastic Moduli of ZnSe

SAMPLE	Elastic Modulus (10^{11} dynes/cm^2) Shear (G*)	Young's (E)	Bulk (K*)
1. Single crystal. (Berlincourt et al., 1963)	2.945	7.57	5.953
2. Single crystal. (Lee, 1970)	2.91	7.54	6.24
3. Single crystal. (Present work)	2.83±0.05	7.39±0.10	6.40±0.06
4. Polycrystalline. (Chung et al., 1967)	2.88±0.07	7.46±0.10	6.67

of Berlincourt's (Table VIII).

5.4 Photoelastic Coefficients

It has been pointed out by Benckert and Bäckström (1973) that it is possible to determine the photoelastic coefficients of transparent crystals by means of Brillouin scattering. In the present experiment the relative magnitude of these coefficients can be estimated from the ratio of peak intensities of the Brillouin components. This ratio may be expressed (Benckert et al., 1973) as a function of the weighting factors $|\underline{\xi}^{\mu}|$ (section 2.5) and the phonon phase velocity (V).

An expression for the relative intensity of the Brillouin components can be developed in the following manner. In the present experiment it was observed that the natural linewidths of the Brillouin components ($\lesssim$ .1GHz) were much less than the instrumental width ($\sim$1.8GHz). This implies that a measure of the integrated intensities of the Brillouin components can, to a good approximation, be replaced by a measure of the peak intensities of these components. The intensity of the scattered field was seen (section 2.6, 2.36) to be proportional to $\langle|\underline{E}'(\underline{K},t)|^2\rangle$ and it follows that the ratio of peak intensities between the Brillouin components of modes μ_1 and μ_2 is given by:

$$\frac{I(\underline{K},\mu_1)}{I(\underline{K},\mu_2)} = \frac{|\underline{\xi}^{\mu_1}|^2}{|\underline{\xi}^{\mu_2}|^2} \frac{\omega^2_{\mu_2}(\underline{K})}{\omega^2_{\mu_1}(\underline{K})}$$

$$= \frac{|\underline{\xi}^{\mu_1}|^2}{|\underline{\xi}^{\mu_2}|^2} \left(\frac{V_2}{V_1}\right)^2$$

where we have used the dispersion relation (2.16).

The ratio $|P_{12}/P_{44}|$ can be obtained from a measure of the peak intensities of the transverse (T_2) and longitudinal(L) phonon modes for the particular scattering geometry ZnSe(110) $X(Z,\frac{Z}{X})Y$. This ratio is given by (Table II):

$$\frac{I(\underline{K},L)}{I(K,T_2)} = \frac{2C_{44}}{C_{11}} \left(\frac{P_{12}}{P_{44}}\right)^2$$

Using the present values for the elastic constants (Table VIII) together with a measure of the relative peak intensities, a suitable weighted average of the results yields:

$$\left|\frac{P_{12}}{P_{44}}\right| = 3.4 \pm 0.3$$

Similarly $|\frac{P_{11}}{P_{12}}|$ may be estimated (Tables III and IV) from the ratio of peak intensities of the longitudinal components from the backscattering geometries: ZnSe(100) $\bar{X}(Z,Z)X$ and ZnSe(110) $\bar{X}(Y,Y)X$. This ratio is:

$$\frac{I(\underline{K}, L_{110})}{I(\underline{K}, L_{100})} = \frac{I_{110}}{I_{100}} \left(\frac{C_{11}}{2(C_{11}+C_{12}+2C_{44})} \right)$$

$$\times \left(\frac{P_{11}}{P_{12}} + 1 - 2\frac{P_{44}}{P_{12}} \right)^2$$

where I_{110} and I_{100} are the incident laser intensities used in the (110) and (100) experiments, respectively. The spectra were performed with different incident power levels and consequently the ratio of peak intensities must be weighted by this factor. The value $\left|\frac{P_{11}}{P_{12}}\right|$ estimated in this manner is :

$$\left|\frac{P_{11}}{P_{12}}\right| = 2.6 \pm 0.2 \quad .$$

5.5 Martin's Consistency Relation

To compare the consistency of the present results with those determined previously by Berlincourt et al. (1963) and Lee (1970) a relationship between the elastic constants due to Martin (1970) is applied. Martin used an expansion of the elastic strain energy in terms of nuclear displacements (Keating, 1966) to develop a relation between the elastic constants. This relation can be expressed as a function of the optic-mode splitting $(\omega_{Lo} - \omega_{To})$, the force constants (k), the equilibrium bond length (r) and the internal-strain parameter (ξ) defined by Kleinman (1962). Using an approximation for the internal-strain parameter suggested by Keating (1966) the relation between the elastic constants and the optic-mode splitting can be written as:

$$\frac{2C_{44}(C_{11}+C_{12}-C')}{(C_{11}-C_{12})(C_{11}+3C_{12}-2C') + 0.831C'(C_{11}+C_{12}-C')} = 1 \qquad (5.1)$$

where $C' = 0.314\ SC_o$

$$S = \frac{(Z^*)^2}{\epsilon} = \left(\frac{\Omega}{4\pi e^2}\right) m\left(\omega_{Lo}^2 - \omega_{To}^2\right)$$

$$C_o = e^2/r^4$$

for the unit cell volume (Ω), the reduced mass (m) and electron charge (e).

Using the value of the optic-mode splitting for ZnSe given by Irwin et al. (1970) the value of S can be determined (S = 0.715). Using the elastic constants determined by Berlincourt, Lee and those of the present experiment the left-hand side of equation 5.1 has been evaluated and the results are given in Table X. Also listed for comparison are values obtained for other similar crystals.

As can be seen from Table X the relation (equation 5.1) between the elastic constants and the optic-mode splitting is not well satisfied using Berlincourt's values for the elastic moduli. Martin (1970) commented that since there is no a priori reason to suspect that ZnSe would be different from similar crystals that this discrepancy would suggest that Berlincourt's value of C_{44} may be in error. This hypothesis has been verified by the present work and as is evident from Table X the present value of equation 5.1 agrees well with the values obtained for similar crystals.

5.6 Neutron Results

The phonon dispersion curves of ZnSe have been measured (Hennion et al., 1971) at room temperature in the [001], [110] and [111] crystallographic directions by inelastic neutron scattering. These dispersion curves can be used to estimate values for the elastic constants which can in turn be compared to previous results. Hennion et al. (1971)

TABLE X

The Value of Martin's Consistency Relation (5.1)

	Material	Left-hand side of Eqn.5.1
1)	ZnSe (Berlincourt et al., 1963)	1.311
2)	ZnSe (Lee, 1970)	1.124
3)	ZnSe (present work)	1.092
4)	ZnS #	1.082
5)	ZnTe #	1.059
6)	AlSb #	1.056
7)	CdTe #	1.045
8)	GaAs #	1.068
9)	GaP #	1.044
10)	GaSb #	1.059
11)	InAs #	1.109
12)	InP #	1.075
13)	InSb #	1.103

Pertinent references given by Martin (1970)

attempted to fit the neutron data with a second-neighbour rigid ion model containing ten general parameters. These parameters were determined by the frequencies of the critical point zone boundary phonons.

The elastic constants were also calculated from the model and an appreciable discrepancy was found between the theoretical value for C_{44} (20.8×10^{10}dyn/cm^2) and that of Berlincourt et al. (44.1×10^{10}dyn/cm^2) (Table XI). Hennion also commented that an increase in the value of C_{11} beyond the experimental limits of Berlincourt's data produced a slight improvement in the match of the data.

Hennion's data was also analyzed by Talwar and Agrawal (1972) with a 7-parameter second-neighbour ionic model (S.N.I.). The model parameters were determined from the measured critical point phonon frequencies and the calculated elastic constants again differed significantly from Berlincourt's. In particular the theoretical value of C_{44} (19.5×10^{10}dyn/cm^2) was similar to that determined by Hennion et al. The results are summarized in Table XI.

On the basis of the above comparison with Berlincourt's results, Talwar and Agrawal suggested that Berlincourt's values were grossly in error and recommended that the elastic constants should be reinvestigated. In view of the results of Lee (1970) and the present work it now appears that Berlincourt's (1963) results were indeed slightly

TABLE XI

Summary of the Elastic Constants of ZnSe

Elastic Constant	Resonance (Berlincourt)	Ultrasonic (Lee)	Brillouin (present)	Neutron (Hennion;Talwar)
C_{11}	81.0±6.0	85.9±0.3	87.2±0.6	84.0 ; 95.7
C_{12}	48.8±6.0	50.6±0.4	52.4±0.8	47.0 ; 51.0
C_{44}	44.1±1.3	40.6±0.2	39.2±0.4	20.8 ; 19.5

in units of 10^{10} dyn/cm^2.

erroneous (5%). However it is also evident that fitting a theoretical model to the neutron data has provided values that are grossly in error (50%). This somewhat limited applicability of rigid ion models has been noted previously. Irwin et al. (1972) commented that such models cannot accurately predict the acoustic modes throughout the Brillouin zone. In particular, if zone boundary frequencies are used to determine the model parameters a good fit will be obtained for large wavevectors but the small wavevector frequencies are highly inaccurate (20-50% error). The present results are further indication of the correctness of this statement.

CHAPTER 6

CONCLUSIONS

6.1 Brillouin Scattering in ZnSe

An apparatus for performing Brillouin scattering measurements has been constructed. The apparatus incorporated a pressure scanned Fabry-Perot interferometer and a single mode of the 514.5 nm line of an Argon-ion laser was used as a light source. The scattered light was detected with a standard photon counting system. To resolve the Brillouin components in the presence of the strong Rayleigh component a molecular iodine filter (Devlin et al., 1971) was used. The filter provided a continuously variable (5~50db) attenuation of the Rayleigh component. As an evaluation of the present experimental technique measurements were performed on α-Quartz for which the elastic moduli are well known. Agreement of the present results with previous measurements has indicated the applicability of the present experimental technique.

The elastic moduli of ZnSe have been determined in the present experiment and present work has confirmed the correctness of previous ultrasonic measurements by Lee (1970). This conclusion is further substantiated from comparisons with the elastic moduli of polycrystalline ZnSe and also

from comparisons with a consistency relation for the elastic constants derived by Martin (1970).

Furthermore, a detailed comparison of the present data with the neutron results has suggested that the SNI model as used by Talwar et al. (1972) yields unreliable values for the phonon frequencies near the center of the Brillouin zone ($\underline{K} = 0$). A similar conclusion was arrived at previously by Irwin and La Combe (1972, 1974) from comparisons of phonon dispersion curves using the SNI model with neutron results and specific heat measurements.

6.2 Suggestions for Future Research

The present research was made possible by the use of a molecular iodine filter (Devlin et al., 1971; Section 3.4) to attenuate the strong Rayleigh component found in the light scattering experiments. However, the accidental coincidence of a Brillouin component with an iodine absorption line resulted in attenuation of the Brillouin component. This problem was evident in the present experiment and served to hinder the measurement of the Brillouin frequency shift.

It would be worthwhile to determine from absorption and fluorescence experiments the distribution and relative intensity of the iodine absorption lines within about 10 cm^{-1} of the tuned argon-ion laser line. A knowledge of the

iodine (I_2) absorption spectra in this region would facilitate the analysis of Brillouin experiments and the absorption lines could also be used as an alternate method for calibration of the Brillouin frequency shifts.

The technique demonstrated in this work should also be ideally suited for the investigation of layer structure semiconductors such as GaSe. These crystals are in general very thin in a direction perpendicular to the layers and as a result ultrasonic techniques are not readily applicable. Brillouin scattering however could be used to measure sound velocities in such crystals and the information gained would be very useful in aiding in an understanding of the effects of the anisotropy in such crystals.

Appendix A

Theory of Elastic Waves in Cubic Crystals

In this section a theory of elastic waves in cubic crystals due to Fedorov (1968) is outlined. The theory is applicable to acoustic vibrations in the long wavelength limit.

If a symmetric stress tensor T is defined such that T_{ij} is the i-th component of the force acting on unit area whose normal has the direction $\hat{\ell}_j$ then, expanding each component of the stress tensor as a Maclaurin series in the deformation:

$$T_{ij} = T_{ij}(0) + \sum_{\ell,m=1}^{3} \left(\frac{\partial T_{ij}}{\partial S_{\ell m}}\right)_{S_{\ell m}=0} S_{\ell m} + \ldots \qquad \text{A1}$$

where $S_{\ell m}$ are the normal strain tensor components (2.6). We assume all deformations $S_{\ell m}$ are small so we need only retain terms up to the first order. The requirement of absolute elasticity implies $T_{ij}(0) = 0$. This simplification results in a linear homogeneous relation between the components of stress and strain (deformation) tensors:

$$T_{ij}(S) = \sum_{\ell,m=1}^{3} \left(\frac{\partial T_{ij}}{\partial S_{\ell m}}\right)_{S_{\ell m}=0} S_{\ell m} \qquad \text{A2}$$

$$= \sum_{\ell,m=1}^{3} C_{ij\ell m} S_{\ell m}$$

where the set $\{C_{ij\ell m}\}$ forms an orthogonal fourth-rank tensor. This relation (A2) is known as the generalized Hooke's law and the coefficients $C_{ij\ell m}$ are referred to as the elastic moduli or elastic constants.

From the symmetry of the stress and strain tensors it follows that the components of the elastic constant tensor obey:

$$C_{ij\ell m} = C_{ji\ell m} = C_{ijm\ell} = C_{\ell mij} \qquad \text{A3}$$

These relations (A3) reduce the number of independent $C_{ij\ell m}$ considerably. It is convenient to pass from the three dimensional fourth-rank tensor to a six dimension matrix representation. This transformation is accomplished by replacing pairs of subscripts with values 1, 2, 3 by one taking on the values 1 through 6 in the following manner:

11 → 1	23 = 32 → 4	A4
22 → 2	13 = 31 → 5	
33 → 3	12 = 21 → 6	

for example: $C_{1111} = C_{11}$, $C_{1223} = C_{64}$

The number of independent $C_{ij\ell m}$ equals the number of independent elements in a six-row symmetric matrix. It further follows from the symmetry of the cubic crystal (Nye, 1957) that :

$$C_{11} = C_{22} = C_{33}\ , \quad C_{44} = C_{55} = C_{66} \qquad \text{A5}$$

$C_{12} = C_{13} = C_{23}$, all other components being identi-

cally zero.

Hence, for the cubic class the six dimensional matrix representation of the elastic constants is given by:

$$(C_{\alpha\beta}) = \begin{pmatrix} C_{11} & C_{12} & C_{12} & 0 & 0 & 0 \\ C_{12} & C_{11} & C_{12} & 0 & 0 & 0 \\ C_{12} & C_{12} & C_{11} & 0 & 0 & 0 \\ 0 & 0 & 0 & C_{44} & 0 & 0 \\ 0 & 0 & 0 & 0 & C_{44} & 0 \\ 0 & 0 & 0 & 0 & 0 & C_{44} \end{pmatrix} \qquad \text{A6}$$

A further restriction on the elastic constants arises from the requirement that the energy associated with the deformation be positive. This implies for the cubic class:

$$C_{11} > |C_{12}| \ , \ C_{11} + 2C_{12} > 0, \ C_{44} > 0 \qquad \text{A7}$$

The general equations of motion follow from equating the i-th component of the force with the acceleration:

$$\rho \ddot{U}_i = \sum_{j=1}^{3} \frac{\partial T_{ij}}{\partial x_j} \quad ; \ i = 1, 2, 3 \qquad \text{A8}$$

Substitution of equations A2 and 2.6 in A8 gives the following wave equation:

$$\rho \ddot{U}_i = \sum_{j,\ell,m=1}^{3} \frac{C_{ij\ell m}}{2} \left[\frac{\partial^2 U_m}{\partial x_j \partial x_\ell} + \frac{\partial^2 U_\ell}{\partial x_j \partial x_m} \right]$$

or equivalently

$$\rho \ddot{U}_i = \sum_{j,\ell,m=1}^{3} C_{ij\ell m} \frac{\partial^2 U_m}{\partial x_j \partial x_\ell} \qquad \text{A9}$$

which follows from the symmetry of $C_{ij\ell m}$ (A3).

We seek travelling wave solutions of the form:

$$\underline{U} = \underline{U}_o \, e^{i(\underline{K}\cdot\underline{r}-\omega t)} \qquad \text{A10}$$

and on substitution in equation A9:

$$\rho\omega^2 U_i = \sum_{j,\ell,m=1}^{3} C_{ij\ell m} \, K_j \, K_\ell \, U_m \qquad \text{A11}$$

where K_j is the j-th component of wavevector $\underline{K}$. In place of $C_{ij\ell m}$ we introduce the reduced elastic modulus tensor $\lambda_{ij\ell m}$:

$$\lambda_{ij\ell m} = \frac{C_{ij\ell m}}{\rho} \qquad \text{A12}$$

and replace K_j by $K(\hat{\ell}_K)_j$ then equation A11 becomes:

$$\sum_{m=1}^{3}\left(\sum_{j,\ell=1}^{3} \lambda_{ij\ell m} \, (\hat{\ell}_K)_j \, (\hat{\ell}_K)_\ell - V^2 \, \delta_{im}\right) U_m = 0 \qquad \text{A13}$$

where δ_{im} is the kronecker delta function and $V = \omega/K$ is the phase velocity.

If we define the second-rank tensor Λ by:

$$\Lambda_{im} = \sum_{j,\ell=1}^{3} \lambda_{ij\ell m} \, (\hat{\ell}_K)_j \, (\hat{\ell}_K)_\ell \qquad \text{A14}$$

then equation A13 becomes:

$$\sum_{m=1}^{3}\left(\Lambda_{im} - V^2 \delta_{im}\right) U_m = 0 \qquad \text{for } i=1,2,3 \qquad \text{A15}$$

This equation (A15) is referred to as Christoffel's equation and is the fundamental eigen-equation for normal mode vibrations in crystalline solids. The square of the phase velocity (V^2) is the root of the characteristic equation:

$$|\Lambda - V^2 \delta_{im}| = 0 \qquad \text{A16}$$

and the eigenvectors ($\hat{U}$) are the unit polarization vectors of the acoustic vibrations.

The problem of determining the normal mode vibrations in an elastic solid reduce to solving for the eigenvectors and eigenvalues of the tensor Λ. The form of this tensor for the cubic class of crystals is given in section 2.7, equation 2.41.

Appendix B

Scattering Coefficient

In this section the present analysis of the scattered field (sections 2.5, 2.6) is compared with the classical treatment of the scattering coefficient. The intensity of the scattered radiation was found (2.24, 2.37) to be proportional to the square of the weighting factor ($|\underline{\xi}|^2$). The magnitude of these factors depends on propagation directions and polarizations of the phonon and photons and on the photoelastic tensor components (2.22 and 2.23).

A comparison between the present formulism due to Benedek and Fritsch (1966) and that of Fabelinskii (1968) can be made in the following manner. The classical scattering coefficient R (Fabelinskii, 1968) is given by:

$$R = \frac{S_n'}{S_n} \left(\frac{L}{V}^2\right) \qquad \text{B1}$$

where S_n and S_n' are the normal components of the Poynting vectors for the incident and scattered waves respectively and L is the length of the scattering medium of volume V. The scattering coefficient R is related to the weighting factor $\underline{\xi}^{\mu}$ in the following manner:

$$R^{\mu}_{\sigma\tau} = \frac{\pi^2 kTn^8}{\rho\lambda^4} \quad \frac{K^2}{\omega_{\mu}^{\ 2}(K)} \; |\underline{\xi}^{\mu}_{\sigma\tau}|^2 \qquad \text{B2}$$

where k is Boltzmann's constant, T the temperature of the medium and the subscripts $\sigma(\sigma = \hat{\ell}_{E_o})$ and τ indicate the polarizations of the incident and scattered waves respectively.

The scattering coefficient (R) and the weighting factor ($\underline{\xi}$) are designated by the phonon mode and by the polarization of the photons. The term $\rho\frac{\omega_{\mu}^{2}(\underline{K})}{K^{2}}$ is only a function of the elastic constants ($C_{\alpha\beta}$) and the factor $\frac{1}{\lambda^{4}}$ is the common Rayleigh scattering factor.

Appendix C

Piezoelectric Stiffening of the Elastic Constants

The effect of piezoelectricity on the measured sound velocities is discussed in this section. Crystals which possess no inversion center are piezoelectric in character. Examples of such crystals are: ZnSe, α-Quartz, CdS and CdSe. The piezoelectric effect associates an induced electric field with a state of deformation of the crystal and it is natural to conclude that the dynamics of such a deformation would be affected by the presence of this induced field. In particular, the phase velocity of the sound wave will depend on its interaction with the field. This piezoelectric contribution to the phase velocity must be considered for any complete theory of Brillouin scattering in piezoelectric crystals.

The effect of piezoelectricity on the velocity of sound waves may be interpreted as a "stiffening" of the elastic constants since the induced electric field acts in such a manner as to oppose the deformation. In the present experiment this was a second order effect since no external D.C. electric field was applied to the crystal. An analysis of the piezoelectric effect follows that given by O'Brien et al. (1969) in which simultaneous solutions to Maxwell's field equations and Newton's second law provides the following

results:

The basic wave equation is the same as that of pure elastic theory (A8):

$$\rho \frac{\partial^2 U_i}{\partial t^2} = F_i = \sum_{j=1}^{3} \frac{\partial T_{ij}}{\partial x_j} \qquad C1$$

where ρ is the mass density, T_{ij} are the stress tensor components. The strain tensor components S_{ij}, are defined in the usual manner (2.6).

For quasi-static fields in non-magnetic, non-conducting, charge free media, Maxwell's equations are given by:

$$\bar{\nabla} \times \bar{E} = 0 \text{ and } \bar{\nabla} \cdot \bar{D} = 0 \qquad C2$$

where $\underline{E}$ is the stress induced internal field and $\underline{D}$ the displacement vector. The fundamental piezoelectric equations for adiabatic conditions are:

$$T_{ij} = \sum_{k,\ell=1}^{3} C^E_{ijk\ell} S_{k\ell} - \sum_{m=1}^{3} e_{mij} E_m \qquad C3$$

and

$$\frac{D_m}{4\pi} = \sum_{i,j=1}^{3} e_{mij} S_{ij} + \sum_{n=1}^{3} \frac{\epsilon_{mn} E_n}{4\pi} \qquad C4$$

where $C^E_{ijk\ell}$ is the elastic constant tensor for constant field, e_{mij} the piezoelectric tensor and ϵ_{mn} the dielectric constant tensor.

Simultaneous plane wave solutions of equations C1 through C4 yields the displacement $\underline{U}$ as solutions to the normal mode equation:

$$\rho\omega^2 U_i = \sum_{j,k,\ell=1}^{3} C^*_{ijk\ell} U_\ell K_j K_k \qquad C5$$

where the "stiffened" elastic constant (in c.g.s.) is given by:

$$C^*_{ijk\ell} = C^E_{ijk\ell} + 4\pi \frac{\sum_{p,q=1}^{3} e_{pij} e_{qk\ell} \hat{K}_p \hat{K}_q}{\sum_{m,n=1}^{3} \epsilon_{mn} \hat{K}_m \hat{K}_n} \qquad C6$$

where $\underline{K}$ is the phonon wave vector with direction cosines $\hat{K}$ ($\hat{K} = \hat{\ell}_K$).

The important result is that the displacement $\underline{U}$ satisfies the same wave equation as in pure elastic theory (A11) with the inclusion of an effective elastic constant $C^*_{ijk\ell}$. The effective elastic constant contains a positive contribution from the piezoelectric effect (if both e's are positive). This "stiffening" of the elastic constant causes the sound velocity to be enhanced and the Brillouin frequency shifts to be increased.

To estimate the importance of the piezoelectric effect in the present experiment on Zinc Selenide, Berlincourt et al.'s (1963) value for the piezoelectric stress tensor components

$e_{14} = e_{25} = e_{36}$ are used ($e_{14} = 0.049$ Coul/m^2). (Note: the crystal symmetry of ZnSe is T_d and thus the only non-zero components are $e_{14} = e_{25} = e_{36}$, where the reduced form $e_{pij} \rightarrow e_{p\alpha}$ has been used (A4)). Using the present value for the elastic constants (Table VIII) and a value of $\epsilon = 6.1$ (Berlincourt et al., 1963) the piezoelectric corrections to the elastic constants are given by the following:

i) the correction to C_{11}:

$$C_{11}^* = C_{11} + \frac{4\pi}{\epsilon} \sum_{p,q} e_{p1}\, e_{q1}\, \hat{K}_p\, \hat{K}_q = C_{11}$$

hence C_{11} is unstiffened (no corrections are required).

ii) the correction to C_{12}:

$$C_{12}^* = C_{12} + \frac{4\pi}{\epsilon} \sum_{p,q} e_{p1}\, e_{q2}\, \hat{K}_p\, \hat{K}_q = C_{12}$$

hence C_{12} is unstiffened.

iii) the correction to C_{44} ($C_{44} = C_{55} = C_{66}$):

$C_{44}^* = C_{44} + \frac{4\pi}{\epsilon} e_{14}^2 (\hat{K}_1)^2$ and since $(\hat{K}_1)^2 \leq 1$ then

$$\frac{C_{44}^* - C_{44}}{C_{44}} \leq \frac{4\pi}{\epsilon C_{44}} (e_{14})^2 \cong 1.14 \times 10^{-3}$$

thus the correction to C_{44} is at most ~.1%.

iv) the correction to the other elastic constants:

By symmetry the only other elastic constants which are stiffened are C_{45}, C_{46} and C_{56} where the stiffening is at most .05% of C_{44}.

Now since the experimental error in this work was of the order of 1% and because the contribution from the piezoelectric effect is at most .1%, the effect of piezoelectric stiffening should be negligible. Furthermore, the results of pure elastic theory (section 2.7; Appendix A) can be used without any modifications to calculate the phase velocity and polarization of the sound waves.

Zinc Selenide is only weakly piezoelectric and no corrections for piezoelectric effects were necessary. However these effects have to be considered in strongly piezoelectric crystals such as α-Quartz. In α-Quartz the only non-zero piezoelectric stress coefficients are e_{11} and e_{14} (Bechmann, 1958). It has been determined that the elastic constant C_{33} is unstiffened for all directions of wave propagation while C_{44} is stiffened only for phonons which have a component of wave propagation normal to the optic axis. Hence for the present backscattering geometry along the optic axis the values obtained for C_{33} and C_{44} (Table VI) need no corrections from piezoelectric effects.

LIST OF REFERENCES

Anderson, O. L. 1963. J. Phys. Chem. Solids 24, 909.

Atanasoff, J. V., and Hart, P. J. 1941. Phys. Rev. 59, 85.

Banerjee, R., and Varshni, Y. P. 1969. Can. J. Phys. 47, 451.

Batchelder, D. N., Collins, M. F., Haywood, B. C. G., and Sidney, G. R. 1970. J. Phys. C, 3, 249.

Bechmann, R. 1958. Phys. Rev. 110, 1060.

Benckert, L., and Bäckström, G. 1973. Phys. Rev. B, 8, 5888.

Benedek, G. B., and Fritsch, K. 1966. Phys. Rev. 149, 647.

Berlincourt, D., Jaffe, H., and Shiozawa, L. R. 1963. Phys. Rev. 129, 1009.

Berlincourt, D. A., Curran, D. R., and Jaffe, H. 1964. In *Physical Acoustics*, edited by W. P. Mason (Academic Press, Inc., New York and London) 1A, 169.

Biondi, M. A. 1956. Rev. Sci. Instrum. 27, 36.

Born, M., and Huang, K. 1954. *Dynamical Theory of Crystal Lattices* (Oxford University Press, New York) p.373.

Brillouin, L. 1914. Compt. Rend. 158, 1331.

Brillouin, L. 1922. Ann. Phys. (Paris) 17, 88.

Cady, W. G. 1964. *Piezoelectricity* (Dover Publications, Inc., New York)

Campbell, J. D., Steinfeld, J. I., and Weiss, N. A. 1969. J. Mol. Spectry. 29, 204.

Cecchi, L., Vacher, R., and Danyach, L. 1970. Le Journal de Physique 31, 501.

Chandrasekharan, V. 1965. Le Journal de Physique 26, 655.

Chung, D. H., and Buessem, W. R. 1967. J. Appl. Phys. 38, 2535.

Damen, T. C., Porto, S. P. S., and Tell, B. 1966. Phys. Rev. 142, 570.

Davis, S. P. 1963. Appl. Opt. 2, 727.

Debye, P. 1912. Ann. Physik 39, 789.

Devlin, G. E., Davis, J. L., Chase, L., and Geschwind, S. 1971. Appl. Phys. Lett. 19, 138.

Fabelinskii, I. L. 1968. *Molecular Scattering of Light* (Plenum Press, New York).

Fedorov, F. I. 1968. *Theory of Elastic Waves in Crystals* (Plenum Press, New York).

Gornall, W. S., and Stoicheff, B. P. 1971. Phys. Rev. B, 4, 4518.

Hennion, B., Moussa, F., Pepy, G., and Kunc, K. 1971. Phys. Lett. 36A, 376.

Hercher, M. 1969. Appl. Opt. 8, 1103.

Huntington, H. B. 1947. Phys. Rev. 72, 321.

Huntington, H. B. 1958. In *Solid State Physics*, edited by F. Seitz and D. Turnbull (Academic Press, Inc., New York) 7, 213.

IRE Standards on Piezoelectric Crystals. 1949. Proc. Inst. Radio Engrs. 37, 1378.

Irwin, J. C., and LaCombe, J. 1970. Can. J. Phys. 48, 2499.

Irwin, J. C., and LaCombe, J. 1972. Can. J. Phys. 50, 2596.

Irwin, J. C., and LaCombe, J. 1974. J. Appl. Phys. 45, 567.

Jenkins, F. A., and White, H. E. 1957. *Fundamentals of Optics* (McGraw-Hill Book Company, Inc., New York) p.283.

Keating, P. N. 1966. Phys. Rev. 145, 637.

Kleinman, L. 1962. Phys. Rev. 128, 2614.

Koga, I., Aruga, M., and Yoshinaka, Y. 1958. Phys. Rev. 109, 1467.

Kurzel, R. B., and Steinfeld, J. I. 1970. J. Chem. Phys. 53, 3293.

Landau, L., and Placzek, G. 1934. Physik Z. Sowjetunion 5, 172.

Lawson, A. W. 1941. Phys. Rev. 59, 838.

Leake, J. A., Daniels, W. B., Skalyo, J., Frazer, B. C., and Shirane, G. 1969. Phys. Rev. 181, 1251.

Lee, B. H. 1970. J. Appl. Phys. 41, 2984.

LeRoi , G., Hatzenbuhler, D., Steinfeld, J. I., and Kurzel, R. B. (unpublished work).

Love, W. F. 1973. Phys. Rev. Lett. 31, 822.

Maradudin, A. A., Montroll, E. W., and Weiss, G. 1963. *Theory of Lattice Dynamics in the Harmonic Approximation* (Academic Press, Inc., New York).

Marple, D. T. F. 1964. J. Appl. Phys. 35, 539.

Martens, F. F. 1901. Ann. Physik 6, 603. In *American Institute of Physics Handbook* (McGraw-Hill Book Company, Inc., Toronto, 1963).

Martin, R. M. 1970. Phys. Rev. B, 1, 4005.

Mason, W. P. 1950. *Piezoelectric Crystals and Their Application to Ultrasonics* (D. Van Nostrand Company, Inc., Princeton, New Jersey).

McSkimin, H. J. 1950. J. Acoust. Soc. Am. 22, 413.

McSkimin, H. J. 1961. J. Acoust. Soc. Am. 33, 12.

McSkimin, H. J. 1962. J. Acoust. Soc. Am. 34, 1271.

McSkimin, H. J. 1964. In *Physical Acoustics*, edited by W. P. Mason (Academic Press, Inc., New York and London) 1A, 271.

Mountain, R. D. 1966. Rev. Mod. Phys. 38, 205.

Nye, J. F. 1957. *Physical Properties of Crystals* (Clarendon Press, Oxford, England).

O'Brien, R. J., Rosasco, G. J., and Weber, A. 1969. In *Light Scattering Spectra of Solids*, edited by G. B. Wright (Springer-Verlag Inc., New York), p.623.

Pecora, R. 1964. J. Chem. Phys. 40, 1604.

Pockels, F. 1906. *Lehrbuch der Kristalloptik* (Teubner, Leipzig). This work described by J. F. Nye, 1957, in *Physical Properties of Crystals* (Clarendon Press, Inc., Oxford, England).

Rambauske, W. R. 1964. J. Appl. Phys. 35, 2958.

Spinner, S., and Tefft, W. E. 1961. Proc. ASTM 61, 1221.

Talwar, D. N., and Agrawal, Bal K. 1972. Solid State Commun. 11, 1691.